Tectonics®

RESEARCH ARTICLE
10.1029/2026TC009404

Key Points:

- West Qinling Mountains record Carboniferous-Triassic deepening from shoal to turbidite fan
- Triassic turbidites were fed from Eurasia with undetected supply from Dabie orogen
- Songpan-Ganzi turbidites accumulated on hyper-extended continental crust, not in remnant ocean basin

Supporting Information:

Supporting Information may be found in the online version of this article.

Correspondence to:

X. Hu,
huxm@nju.edu.cn

Citation:

Pan, Y., Hu, X., Garzanti, E., Ma, A., & Deng, T. (2026). The tectonic debate on the Songpan-Ganzi domain: Remnant ocean basin or hyper-extended continental margin? *Tectonics*, *45*, e2026TC009404. https://doi.org/10.1029/2026TC009404

Received 5 FEB 2026
Accepted 20 OCT 2026

Author Contributions:

Conceptualization: Yingdi Pan, Xiumian Hu
Data curation: Yingdi Pan, Xiumian Hu, Anlin Ma, Tao Deng
Formal analysis: Yingdi Pan, Eduardo Garzanti
Funding acquisition: Xiumian Hu
Investigation: Yingdi Pan, Eduardo Garzanti, Anlin Ma, Tao Deng
Methodology: Yingdi Pan
Project administration: Xiumian Hu
Resources: Xiumian Hu
Supervision: Xiumian Hu
Validation: Xiumian Hu
Visualization: Yingdi Pan
Writing – original draft: Yingdi Pan
Writing – review & editing: Yingdi Pan, Xiumian Hu, Eduardo Garzanti, Anlin Ma, Tao Deng

© 2026 American Geophysical Union. All rights reserved, including rights for text and data mining and training of artificial intelligence technologies or similar technologies.

The Tectonic Debate on the Songpan-Ganzi Domain: Remnant Ocean Basin or Hyper-Extended Continental Margin?

Yingdi Pan[1], Xiumian Hu[1], Eduardo Garzanti[2], Anlin Ma[1], and Tao Deng[1]

[1]State Key Laboratory of Critical Earth Material Cycling and Mineral Deposits, MOE Key Laboratory of Surficial Geochemistry, School of Earth Sciences and Engineering, Nanjing University, Nanjing, China, [2]Laboratory for Provenance Studies, Department of Earth and Environmental Sciences, Università di of Milano–Bicocca, Milano, Italy

Abstract The Triassic Songpan-Ganzi basin, located in northeastern Tibet, is one of the world's largest preserved ancient deep-marine siliciclastic basins, yet its tectonic origin remains contentious. While often regarded as a remnant-ocean basin, it has also been interpreted as a stretched and thinned continental margin. To resolve this debate, we investigated the basin's northeastern side in the West Qinling Mountains through integrated stratigraphic, sedimentological, petrographic, heavy-mineral, and detrital zircon U-Pb analyses. Our results show deepening from coastal depositional environments in the Early Carboniferous to widespread submarine-fan sediments in the Middle Triassic. The Triassic deep-sea turbidites were mainly sourced from the southern North China block, including the East Kunlun, Qilian, and Qinling orogens, rather than from the eastern Dabie orogen. These findings support the interpretation that the Songpan-Ganzi region represents the hyper-extended continental margin of the North China block rather than a remnant-ocean basin. Such a revised tectonic framework has major implications: it redefines the Triassic magmatism in the Songpan-Ganzi basin as post-collisional rather than related to oceanic subduction and, critically, explains the high thermal gradients and extensive fault networks typical of extensional settings that favored the formation of the region's world-class Carlin-type gold deposits.

Plain Language Summary The Songpan-Ganzi basin in northeastern Tibet contains one of the world's largest and best-preserved accumulations of ancient deep-sea sedimentary rocks. For a long time, geologists have debated how this basin was formed: some viewed it as an ancient ocean trapped between colliding continents, while others interpreted it as a stretched and thinned part of the continental margin of the North China block. To test these contrasting hypotheses, we studied rocks from the basin's northeastern edge in the West Qinling Mountains. Our results show that between the Carboniferous and Triassic periods this area gradually subsided from a coastal environment to a deep-sea setting. The sediments that filled the deep basin were mostly eroded from mountain belts to the north—the East Kunlun, Qilian, and Qinling ranges—with undetected contribution from the Dabie Mountains to the east. These findings indicate that, during the Triassic, the Songpan-Ganzi region was not a remnant ocean basin trapped between colliding continents but represented a stretched, submerged part of the southern North China block. This conclusion helps clarify the tectonic architecture of geological terranes issued from the old Paleotethys Ocean that now constitute the northeastern Tibetan Plateau, as well as the origin of Triassic world-class gold deposits.

1. Introduction

The Songpan-Ganzi basin is one of the largest turbiditic submarine fans on Earth, covering ~200,000 km^2 of the eastern Tibetan Plateau with a volume of ~2.0×10^6 km^3 (Nie et al., 1994; Xu et al., 1992; A. Yin & Nie, 1993). According to the predominant view, the Songpan-Ganzi domain was a remnant-ocean basin during the diachronous Triassic collision between the South China and North China blocks, as suggested by studies in the West Qinling Mountains to the northeast of the basin (Nie et al., 1994; Zhou & Graham, 1995). The main supporting evidence includes: (a) sediment primarily derived from the Qinling-Dabie orogenic belt; (b) great thickness of Triassic deep-sea sediments and occurrence of mafic-ultramafic rocks along fault zones (e.g., Xianshuihe fault) suggesting the possibility of an oceanic basement (de Sigoyer et al., 2014; S. Y. Song et al., 2004; Sengör, 1984; Şengor & Hsü, 1984). The provenance of Triassic turbidites was inferred based on: (a) southward to southwestward paleocurrent directions; (b) transition from Lower Triassic pelagic limestones to olistostromal deposits containing clasts of Paleozoic shelf carbonates, overlain in turn by Middle Triassic deep-sea turbidites supposedly

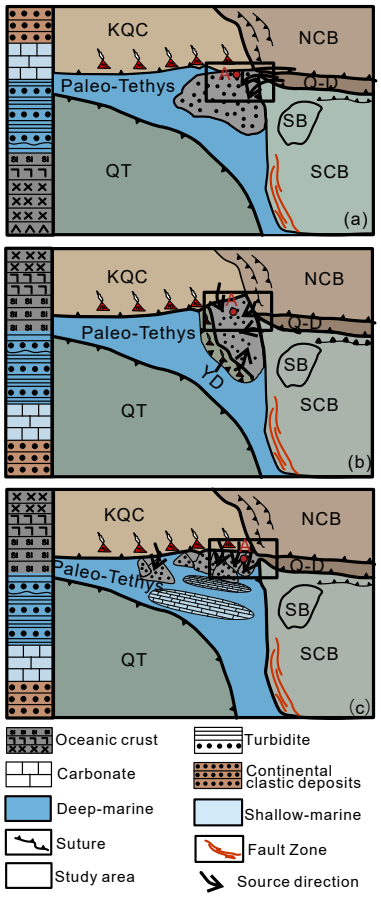

Figure 1. Alternative paleogeographic models for Triassic Songpan-Ganzi turbidites: (a) remnant ocean basin (mod. after Weislogel et al., 2010); (b) Mediterranean-type back-arc basin (mod. after Pullen et al., 2008); (c) continental extensional basin (mod. after E. Z. Chang, 2000). Stratigraphic columns depict the theoretical stratigraphic sequences expected for the three evolutionary models at Area A. NCB: North China block; KQC: East Kunlun-Qilian-Qaidam terranes; Q-D: Qinling-Dabie orogenic belt; QT: Qiangtang block; SB: Sichuan basin; SCB: South China block; YD: Yidun arc.

reflecting the progressive unroofing of the Qinling–Dabie belt; (c) comparable volumes of Triassic Songpan-Ganzi sediments and of material eroded from the Qinling-Dabie belt (Figure 1a; Nie et al., 1994); (d) age spectra of detrital zircons in Triassic turbidites consistent with zircon-age data from the Qinling-Dabie belt (Enkelmann et al., 2007; Jian et al., 2019; Tang et al., 2023; Weislogel et al., 2006, 2010).

The Songpan-Ganzi has been alternatively envisaged as a continental extensional basin (Figure 1c; E. Z. Chang, 2000; B. W. Chen et al., 1987; S. N. Liu & Wang, 2023; Meng & Zhang, 1999; Zhan et al., 2021; Q. Zhang et al., 1994) based on the following lines of evidence: (a) fauna and flora of Yangtze block affinity contained in Neoproterozoic-Paleozoic strata of the North Songpan, Muli, and Batang regions (E. Z. Chang, 2000); (b) geochemistry and geochronology of the Middle–Upper Permian volcano-sedimentary succession in the Songpan-Ganzi basin (Danba-Xiaojin area) comparing well with rift sequences in the western Yangtze block (Panxi region; S. N. Liu & Wang, 2023); (c) paleocurrents in the West Qinling Mountains changing from mostly northward in the Lower Triassic to mainly southward in the Middle Triassic (L. Li et al., 2014); (d) U–Pb ages of zircons in granitoid rocks intruding the Triassic turbidites ranging from 250 to 234 Ma (L. Li et al., 2014).

As a further option, the Songpan-Ganzi basin was considered to be a Mediterranean-type back-arc basin formed behind the Yidun arc during subduction and roll-back of Paleotethyan oceanic lithosphere (Figure 1b; Burchfiel et al., 1995; Pullen et al., 2008; L. Li et al., 2014). Further studies, however, highlighted that quasi-aluminous, high-potassium, calc-alkaline magmatic rocks of the "Yidun Arc," dated as Late Triassic-earliest Jurassic, range from collisional to post-collisional, thus refuting the key evidence for this model (X. Hu et al., 2026; Zhan et al., 2021).

Previous provenance studies tried to solve the controversy, but in the absence of a systematic stratigraphic analysis they produced conflicting evidence concerning paleocurrents and age spectra of detrital zircons. To achieve an accurate reconstruction of the basin's stratigraphy and a comprehensive evaluation of provenance data we conducted integrated sedimentological, petrographic, heavy-mineral, and detrital-zircon geochronological analyses of Carboniferous–Triassic strata in the West Qinling Mountains. The results offer new constraints on the tectonic setting of the Songpan-Ganzi basin.

2. Geological Framework

2.1. Tectonic Setting of the West Qinling Mountains

The Songpan-Ganzi basin is bounded by the East Kunlun-Qilian-Qaidam terranes (KQC) and the North China block to the north, by the Qiangtang and Yidun terranes to the south, and by the Longmenshan thrust belt and South China block to the east (Nie et al., 1994; Xu et al., 1992; A. Yin & Harrison, 2000). The thick Triassic deep-sea turbidites it contains, along with the underlying basement and overlying sedimentary sequences, underwent intense deformation in the Late Triassic (Figure 2a; E. Z. Chang, 2000; Nie et al., 1994; Xu et al., 1991). The Neoproterozoic granitoid basement and stratigraphically overlying Paleozoic strata exposed along the perimeter of the Songpan-Ganzi basin show petrological and geochemical affinities with the South China block (E. Z. Chang, 2000; S. N. Liu & Wang, 2023). This is evidence of deposition on continental (possibly a continental ribbon) rather than oceanic crust, although the westward extension of Precambrian basement is unknown.

The northeasternmost exposure of Triassic Songpan-Ganzi deep-sea sediments is located in the West Qinling Mountains (Figure 2a), separated from the Bayankhara depocenter by the Mianxian-Bashan fault (Figure 2a). Because of uncertainties in stratigraphic age, previous studies either considered these two regions as tectonically

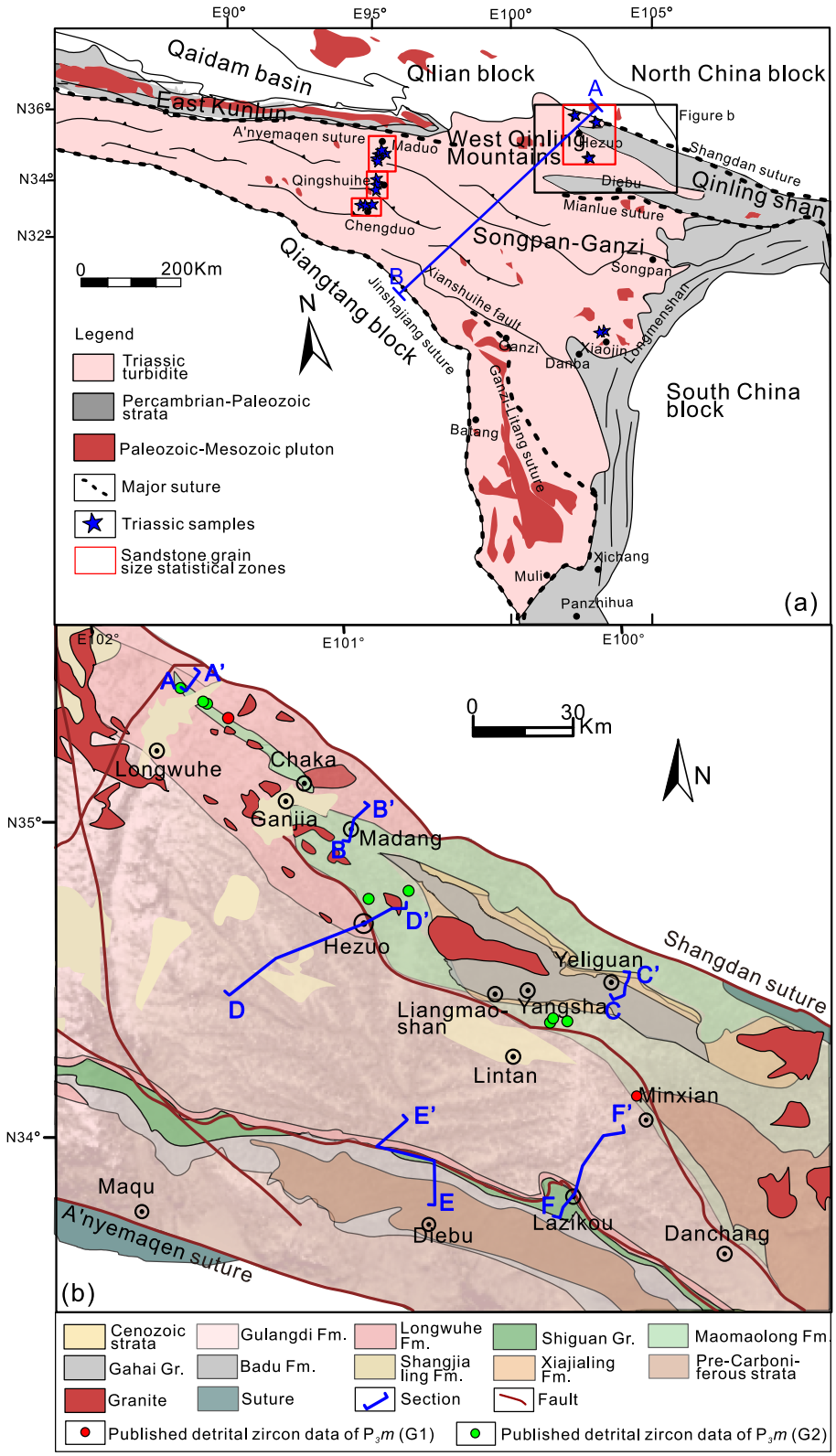

Figure 2. Tectonic map of Songpan-Ganzi basin and surrounding terranes ((a); mod. after Weislogel et al. (2010); (b)) simplified geological map of West Qinling Mountains (mod. after BGMRGS, 1989). Fm. = Formation; Gr. = Group.

distinct domains (T. T. Wang et al., 2024) or interpreted the West Qinling Mountains as thrust nappes derived from the main Songpan-Ganzi basin (Nie et al., 1994; Zhou & Graham, 1995). Recent studies, however, showed that the collision between the South China and North China blocks occurred before the Permian, and that no ocean existed between them in the Permian to Triassic (Cheng & Cao, 2015; Deng et al., 2024; X. C. Liu et al., 2011; Z. Q. Liu et al., 2011; Shi et al., 2022; Tang et al., 2023).

2.2. Stratigraphy of the Northern West Qinling Mountains

The Carboniferous-Triassic strata exposed in the northern West Qinling Mountains include the Badu, Xiajialing, Shangjialing, Daguanshan, Maomaolong, Longwuhe, and Gulangdi formations (Figure 2b; BGMRGS, 1989; Feng et al., 2003). The Badu Fm. mostly consists of siliciclastic rocks locally intercalated with carbonate layers containing brachiopods (*Chonetes sp.*) and foraminifera (*Eostaffella sp.*) of Early Carboniferous age (Figure 2b; BGMRGS, 1989; Cao et al., 1995; Gao, 2019; Yin, 1992). Exposed in the Yangsha area are mostly massive to thick-bedded, greenish-grey fine sandstones with minor intercalations of purple mudrocks, commonly displaying fining-upward sequences with well-developed parallel and oblique lamination. Sedimentological evidence suggests a subaerial delta-plain environment.

The Xiajialing Fm., regionally exposed along a narrow WNW-trending belt in fault contact with the Badu Fm., consists of grey-black bioclastic limestone, gravelly limestone, and siltstone in the Yeliguan area. Carbonate layers commonly contain mm- to cm-sized terrigenous grains. Bioclasts are mainly echinoderms with bivalves, gastropods, and benthic foraminifera. Fusulinids including *Schubertella obscura*, *Fusulinella sp*., and *Eostaffella sp.* indicate a mid-Carboniferous age (BGMRGS, 1989; Yin, 1992). Deposition in a semi-restricted platform to platform-margin shoal is indicated (BGMRGS, 1989; Gao, 2019).

The Shangjialing Fm., unconformably overlying the Xiajialing Fm., mostly consists of massive to thick-bedded bioclastic limestone with algae, bryozoans, echinoderms, and foraminifers in the Yeliguan area. The fusulinid assemblage (BGMRGS, 1989) constrains the depositional age as Late Carboniferous. Deposition occurred on a semi-restricted carbonate platform.

The overlying Daguanshan Fm. consists of limestone, siltstone, and sandy mudrock. The thick limestone intervals in the Longwuhe area yielded calcareous sponges, calcareous algae, corals, bryozoans, fusulinids and other foraminifera, constraining the depositional age as Early-Middle Permian (Kou et al., 2009; Yin, 1992).

The Maomaolong Fm. mainly consists of sandstones and mudrocks interbedded with pebbly sandstones and conglomerates (BGMRGS, 1989). Abundant fossil fragments range in age from the Carboniferous to the Early Permian (Jin & Li, 1995; L. Li et al., 2014; Yin, 1992).

The Longwuhe and Gulangdi formations consist of conglomerates, pebbly sandstones, sandstones and mudrocks. Sole marks and graded bedding followed by parallel lamination and ripples indicate turbiditic deposition. Incomplete Bouma sequences and slumps are common. Fossils in the intercalated marly intervals are mainly Triassic ammonites and bivalves (BGMRGS, 1989; Meng et al., 2007; Yan et al., 2020; Y. X. Zhang et al., 2014).

2.3. Stratigraphy of the Southern West Qinling Mountains

In the southern belt of the West Qinling Mountains, Devonian siliciclastic rocks and carbonates rest upon Silurian turbidites and carbonates. Lower Devonian sandstones and carbonates containing ostracods, lamellibranchs, brachiopods, corals and plant fossils were deposited in delta-plain to tidal flat environments. The Middle Devonian Dangduogou Formation consists of glauconite-bearing siliciclastic rocks with minor carbonates, whereas the Gudaoling Formation comprises carbonates overlain by siliciclastic rocks. Both formations contain brachiopods and corals, and are characterized by common siderite nodules and hematite interlayers. The Upper Devonian Tieshan Group is dominated by carbonates with abundant brachiopods. Middle to Upper Devonian deposits display ripples, wavy and flaser bedding, basal erosion structures and bioherms indicating a shallow-marine environment (BGMRGS, 1989; Yan et al., 2016).

Most Carboniferous strata in the southern belt of the West Qinling Mountains are shallow-marine limestones rich in corals, brachiopods, and foraminifera. The Lower Carboniferous Yiwa Fm. mostly consists of medium- to thick-bedded limestones with local chert nodules and bands, with medium-bedded dolostones in the middle part. The Lveyang Formation mainly consists of limestone, locally with marl or siltstone interbeds. The Middle

Carboniferous Minhe Fm. is composed of thick-bedded limestones, rich in fusulinids and corals. The Upper Carboniferous Gahai Group consists of thick-bedded limestones, separated from the underlying strata by a basal calclithitic conglomerate. All of these Carboniferous strata were deposited in a shallow-marine environment (BGMRGS, 1989).

The shallow-marine Permian succession includes the Lower Permian Daguanshan and Upper Permian Shiguan groups (BGMRGS, 1989). The Daguanshan Group mostly consists of medium- to thick-bedded gray limestones locally intercalated with thin-bedded marls, and contains abundant fusulinids. The Shiguan Group begins with a succession of organic-rich siliciclastic rocks, overlain by thin-bedded to massive gray limestones.

The Triassic succession includes the Longwuhe and Gulangdi formations but with markedly different lithofacies from those of the northern belt. The Lower Triassic Longwuhe Formation is dominated by limestones and minor marls containing lamellibranchs. The Gulangdi Formation is characterized by limestones in the lower part and by interbedded limestones, mudrocks, and sandstones yielding brachiopods, gastropods, and plant fragments in the upper part (BGMRGS, 1989). Sole marks and incomplete Bouma sequences indicate turbiditic deposition.

2.4. Stratigraphy of the Central Songpan- Ganzi Basin

The central Songpan-Ganzi Basin is characterized by an enormously thick succession of Triassic turbidites, known as the Bayankhara Group in Qinghai Province. This very thick unit, monotonously consisting of turbiditic sandstones and mudrocks with minor calcareous and volcanic components, is subdivided into four units (from base to top): (a) interbedded sandstone and mudrock; (b) sandstone; (c) claystone; (d) sandstone. Bivalves and ammonites occur (BGMRGS, 1989).

2.5. Structure and Magmatism of the West Qinling Mountains

From north to south, the WNW-trending West Qinling Mountains include the Wushan–Tianshui, Xiahe–Lixian, Luqu–Chengxian, Diebu–Wudu, and Maqu–Nanping–Wenxian thrust-nappe belts, folded in the Lixian–Xiahe overturned plunging anticline, Luqu–Chengxian overturned syncline, and Bailongjiang plunging anticline (Feng et al., 2002). Well-preserved large-scale extensional structures are lacking, possibly masked by subsequent strong overprint during the Late Triassic Indosinian collisional orogeny.

Extensive magmatism began at the end of the Permian (~254 Ma) and persisted through most of the Triassic (until ~210 Ma) (F. Y. Hu et al., 2020). Zircon U-Pb geochronology indicates that granodiorites and granites were emplaced mainly between 245 and 235 Ma in the west, and between 230 and 210 Ma in the east (Table S5; Dou et al., 2019; Han et al., 2024; Luo et al., 2012; Qiu et al., 2016). Most granitoids have metaluminous affinity and are classified as I-type (X. W. Li et al., 2015; H. N. Liu et al., 2021; Qiu & Deng, 2017; X. X. Wang et al., 2013); several plutons contain abundant mafic microgranular enclaves (Han et al., 2024). Mafic to ultramafic rocks, commonly emplaced as dikes or lenses into the turbiditic succession along NWW-trending fault zones, are dated as Late Permian to Early Triassic in the Longwuhe, Ganjia, and Liangmaoshan areas (Table S5; L. Li et al., 2014; H. Q. Wang et al., 2010).

2.6. The A'nyemaqen Suture Zone

The A'nyemaqen Suture Zone is bounded to the north by the East Kunlun Orogenic Belt and to the south by the Bayankhara terrane. It extends westward from the Altyn Tagh Fault in the west through the A'nyemaqen Mountains to the Qinling Orogenic Belt in the east, with a total length exceeding 1,000 km (Figure 2a). The suture zone contains typical ophiolitic suites, including ultramafic rocks, gabbro, basalt, and abyssal siliceous rocks. Isotopic ages of gabbro and basalt (333–308 Ma) indicate that the A'nyemaqen Ocean opened at least as early as the Early Carboniferous (Z. Q. Liu et al., 2011; J. S. Yang et al., 2009). The Buqingshan Group, a tectonic mélange exposed in the suture zone, is subdivided into the Shuweimenke and the Maerzheng formations. The former is dominated by shallow-water carbonates containing Middle Permian fusulinids, brachiopods, and rugose corals, representing a platform environment during the early stage of oceanic expansion. The latter consists of slate, reddish siliceous shale, and chert rich in radiolaria, indicating continuing basin expansion and deepening during the Early to Middle Permian (Z. Q. Liu et al., 2011; Zhao et al., 2013, 2016). The timing of the final closure of the A'nyemaqen Ocean remains controversial. Some researchers underscore the presence of an angular unconformity between Upper Permian and underlying strata, thus arguing for a Late Permian closure (R. B. Li

et al., 2012). Others favor an Early Triassic closure, based on the transition from deep-water to shallow-water sedimentary facies, the significant difference in Middle Triassic ammonoid faunas between the northern and southern sides of the suture, and the occurrence of Upper Permian island-arc volcanic rocks as well as Lower–Middle Triassic back-arc-basin basalts (J. S. Yang et al., 2009). Kong et al. (2020) and F. C. Wang et al. (2023) identified Middle Triassic (ca. 247–238 Ma) granites with adakitic characteristics (high Sr/Y and La/Yb ratios), suggesting that the A'nyemaqen Ocean closed in the Middle Triassic. Moreover, other researchers consider all Triassic granites to be products of arc magmatism, implying that the ocean basin may have persisted until the Late Triassic (Q. F. Ding et al., 2014). Further evidence is therefore needed to better constrain the final closure of the A'nyemaqen Ocean within the wide Late Permian to Late Triassic time window.

3. Samples and Methods

Five stratigraphic sections along a south-to-north profile were measured in the West Qinling Mountains, describing sedimentary textures and structures, conglomerate-clast composition, and limestone microfacies. Stratigraphic and sedimentological observations were also made in the Chaka, Yangsha and Yeliguan areas (Figure 2b). In addition, 24 Triassic samples were collected from the Bayankhara area (Figure 2a). Sampling locations are shown in Figure 3 and Table S1.

3.1. Sandstone Petrography and Heavy Minerals

A total of 88 Carboniferous to Triassic sandstones were analyzed by counting ~400 grains per thin section following the Gazzi-Dickinson method (Ingersoll et al., 1984; sandstone classification after Garzanti, 2019). On each of 58 Lower to Middle Triassic sandstones, the maximum apparent diameter D of ≥200 grains (mm; converted in Φ units as $-\log_2 D$) was measured under a polarizing microscope using *Nikon NIS Elements* software for image analysis. Graphic methods were employed to calculate the median (D_{50}) and mean grain size of each sample (Table S3).

From a split aliquot of the sieved 32–500 μm fraction of 27 selected samples, heavy minerals were separated by centrifuging in Na-polytungstate (2.90 g/cm^3), recovered by partial freezing with liquid nitrogen, and mounted on a slide using Canada balsam. At least 200 non-opaque grains were counted under the optical microscope at an appropriate regular spacing (Garzanti & Andò, 2019). The GPS coordinates of sample localities and point-counting results are presented in Table S2.

3.2. Zircon U-Pb Dating

Zircon grains separated by elutriation and magnetic methods from 11 sandstones, one sandstone pebble, and three igneous rocks were hand-picked, mounted, and polished to expose grain interiors. Sample 23WQL55, three igneous rocks, and 79 zircon grains from sample 23WQL68 were dated with an Agilent 7500a laser inductively coupled plasma mass spectrometer (LA-ICP-MS) at the Nanjing Hongchuang Geological Exploration Technology Service Co., Ltd. (NHEXTS), Nanjing, China. Analyses were conducted with laser beam diameter 25 μm, repetition rate 7 Hz, and energy density 7 J/cm^2. The other samples were analyzed for U-Th-Pb elements by an ICP-MS Agilent 7500a, equipped with a GeoLas Pro 193 nm laser ablation system, at the State Key Laboratory of Critical Earth Material Cycling and Mineral Deposits, Nanjing University, following Jackson et al. (2004). A laser beam diameter of 29 μm was used, with frequency 5 Hz, and energy density 3.28 J/cm^2. The zircon standard GEMOC GJ-1 (^{207}Pb/^{206} Pb age 608.5 ± 1.5 Ma; Jackson et al., 2004) was used as external reference material. The secondary standard 91500 (^{206} Pb/^{238} U TIMS age 1,065.4 ± 0.6 Ma, Wiedenbeck et al., 2004) was analyzed during every U–Pb run for quality control, yielding a weighted average ^{206}Pb/^{238}U age of 1,060.6 ± 1.2 Ma. ^{206}Pb/^{238}U ages were selected for zircon grains younger than 1,000 Ma and ^{207}Pb/^{206}Pb ages for grains older than 1,000 Ma, neglecting grains with >10% discordance for ages >400 Ma (Gehrels et al., 2008). Overall, a total of 1,036 concordant detrital zircon ages and 29 magmatic zircon ages were obtained. The toolset *detritalPy* was used to generate histograms and kernel density estimates (Sharman et al., 2018). Data are reported in Table S4.

For provenance comparison, we compiled detrital-zircon age data from all potential source terranes (East Kunlun-Qilian-Qaidam, Qinling, southern North China block, South China block, Qiangtang block) and from Silurian to Triassic strata of the West Qinling Mountains (Y. D. Pan & Hu, 2024). Data for the Bayankhara Group between longitude 95°E and 100°E are also from Y. D. Pan and Hu (2024) (Table S6). Maximum depositional ages were

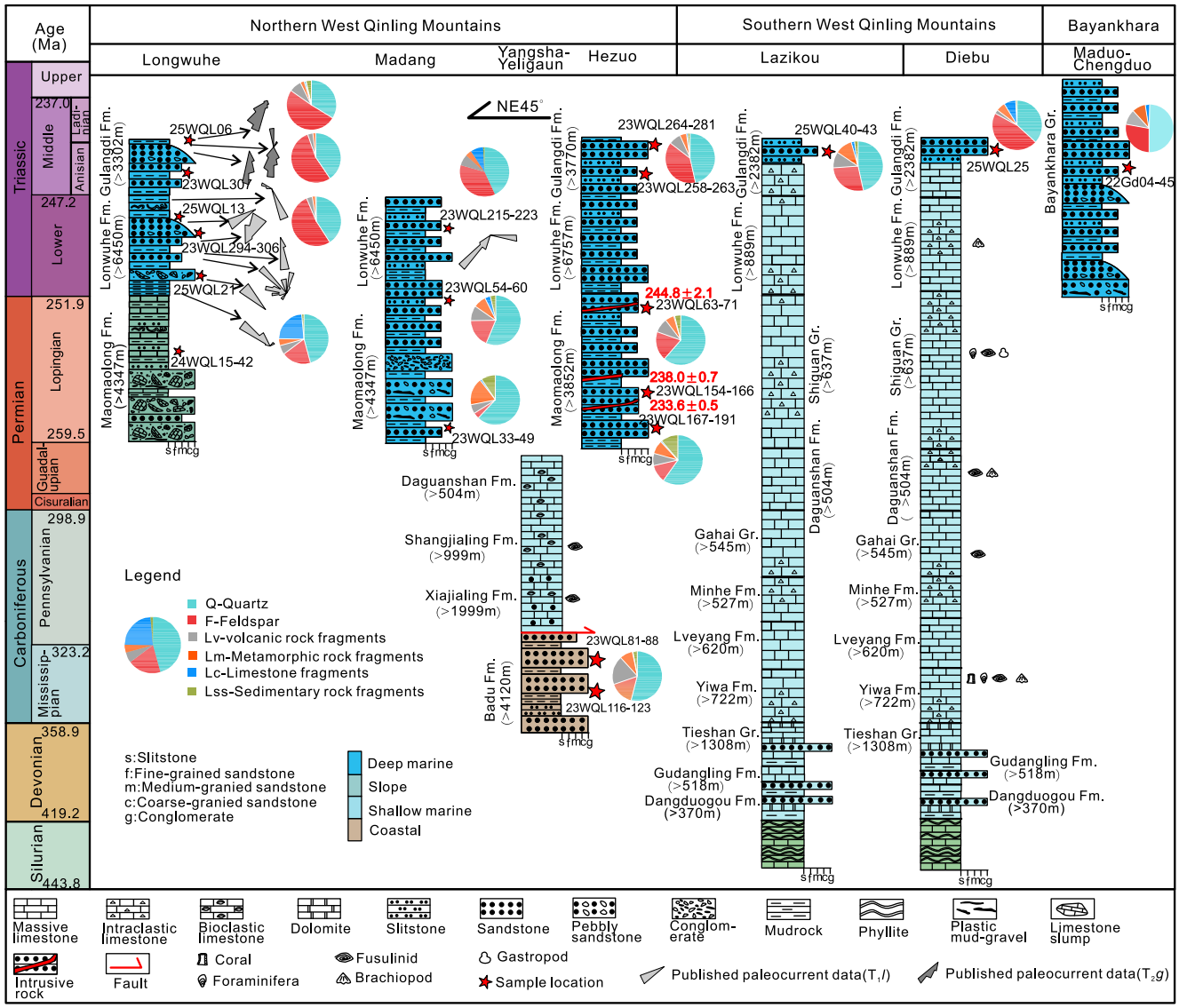

Figure 3. Stratigraphic logs in West Qinling Mountains and Bayankhara area. Late Permian: continental slope facies characterized the Longwuhe and Chaka areas, and submarine-fan deposits the Hezuo and Madang regions in the middle of the basin. Early Triassic to Middle Triassic (early Anisian): turbiditic deposition was widespread, excepting the southern Diebu and Lazikou areas where shallow-marine carbonates deposited from Carboniferous to early Anisian passed to semi-deep- to deep-marine turbidites in late Anisian time.

calculated following Dickinson and Gehrels (2009), Coutts et al. (2019), and Vermeesch (2021), with a preference for Y1δ (2+) ages (weighted mean age ±1σ incorporating both internal analytical error and external systematic error; Table S7).

Three-dimensional metric multidimensional scaling (MDS) was used to compare detrital-zircon U-Pb age distributions (Vermeesch, 2013). Pairwise dissimilarities were quantified using the two-sample Kolmogorov-Smirnov statistic (*D*), defined as the maximum absolute difference between the empirical cumulative distribution functions of two age data sets. Smaller D values indicate more similar age distributions. The resulting dissimilarity matrix was used as input for three-dimensional metric MDS in Python using scikit-learn, with a fixed random seed of 42 and a maximum of 1,000 iterations.



Figure 4. Field photographs from West Qinling Mountains (a–h) and Bayankhara area (i–j). Maomaolong Fm. (a–f): (a) Longwuhe section; (b) soft-sediment deformation (Longwuhe section); (c) flute casts (Hezuo section); (d) conglomerates interbedded with slumped limestone layer with poor lateral continuity (Chaka area); (e) turbidite intruded by granite porphyry dated as 244.8 ± 2.1 Ma (Hezuo section); (f) soft-sediment deformation (Chaka area). Gulangdi Fm.: (g) massive shallow-marine limestone in fault contact with calcareous sandstone (Diebu section). Longwuhe Fm.: (h) conglomerate (Longwuhe section). Bayankhara Gr.: (i) turbidites; (j) incomplete Bouma sequences.

4. Results

4.1. Facies Analysis

4.1.1. Maomaolong Formation

In the Longwuhe section, the 1000-m-thick Maomaolong Fm. lies in fault contact with the Longwuhe Fm. (Figure 3). The up to 350-m-thick lower part mostly consists of conglomerate and breccia interbedded with thin to medium sandstone layers. Dominant carbonate clasts, centimeters to meters in size and very poorly sorted, consist of light grey shallow-water carbonate containing Late Carboniferous to Early– Middle Permian fusulinids and corals; quartz grains are minor. Deposition took place by submarine rockfall, avalanching, or slump (Figure 4a).

The up to 650-m-thick upper part mainly consists of rhythmically alternating fine sandstone-siltstone-marl-thin limestone intervals comparable to Tc-Te Bouma sequences (Bouma, 1964) (Figure 4a). Soft-sediment deformation is widely observed in both sandstone and mudrock layers (Figure 4b). Deposition took place in a low-energy, distal or marginal part of a turbidite system or submarine channel-levee complex (Cronin, 2018; Mutti, 1985). Slope and submarine-fan environments are indicated.

In the Chaka area, the unit mainly consists of poorly sorted conglomerate with slumped limestone blocks (Figure 4d), subangular to subrounded clasts ranging in size up to 30 cm and including limestone, quartz, and minor granite. Soft-sediment deformation structures are widespread in the limestone (Figure 4f). The Nereites ichnofacies (Jin & Li, 1995) includes *Cosmorhaphe*, *Helminthopsis, Helminthoida, Megagrapton, Scolicia, Neonereites*. A deep-water (slope) facies is indicated.

In the Madang section, the unit consists of interbedded fine sandstone and mudrock. Sandstone layers display erosional base with sole marks and horizontal to ripple lamination. Poorly sorted conglomerates locally displaying inverse grading may occur with limited lateral continuity. Submarine-fan channel and lobe environments are indicated.

In the Hezuo section, the lower part of the unit consists of thin- to medium-bedded fine sandstone interbedded with mudrock (Figure 4c). Coarse sandstones with erosional base, load casts, plastic mudclasts, and incomplete Bouma sequences occur locally, pointing to fan lobe environments. The upper part of the unit mostly consists of thin-bedded siltstones with flute casts (Figure 4e). Deposition by hemipelagic suspension in submarine fan fringe environments is indicated.

4.1.2. Longwuhe Formation

In the Longwuhe section, the unit mostly consists of poorly sorted conglomerate and pebbly sandstone with poor lateral continuity (Figure 4h). Subrounded clasts range up to 30 cm in size. Rip-up mudclasts up to 10 cm in size and displaying soft sediment deformation occur at the base of some layers, commonly aligned parallel to bedding. Flame or loading structures and incomplete Bouma sequences are observed. Proximal fan to fan-channel environments are indicated.

In the Madang section, the unit displays two distinct facies. The first facies consists of mudrock and up to 12-cm-thick sandstone layers showing sharp base, normal grading, well-developed parallel and ripple lamination, and gradational top. Common injection or flame structures indicate soft-sediment deformation. A distal or marginal, low-energy part of a turbidite system is indicated (Cronin, 2018; Mutti, 1985). The second facies consists of thin bedded, laterally continuous micritic limestone locally interbedded with mudrock, indicating dominant pelagic settling. Overall, a bathyal to abyssal environment is suggested.

In the Hezuo section, the unit exhibits the same two facies described above but also includes medium- to thick-bedded sandstones with erosional base, sole marks, and normal grading. Turbidite channel or proximal lobe facies in a submarine fan are indicated.

In the Diebu and Lazikou sections, the unit mainly consists of thin- to medium-bedded grey or red limestone, bioclastic limestone with fusulinids and brachiopods, and mudrock. A shallow-marine environment is suggested.

4.1.3. Gulangdi Formation

In the Longwuhe section, the unit mostly consists of conglomerate, sandstone, and mudrock. Poorly sorted conglomerates with limited lateral continuity and containing angular to subangular clasts up to 30 cm in diameter suggest deposition in a proximal turbidite fan. Mudrocks interbedded with 10–20 cm-thick sandstones with erosional base, sole marks, and Td-Te Bouma sequences point at distal submarine-fan lobe environments. Very thin mudrock interlayers document hemipelagic deposition. Bathyal to abyssal environments are indicated.

In the Hezuo section, the unit consists of sandstones with erosional base, sole marks and normal grading, interbedded with mudrocks showing flame structures. A ∼40-m-thick massive coarse sandstone with graded bedding and limited lateral continuity occurs in the middle part of the section. Overall, deposition in submarine channels and fan lobes is indicated.

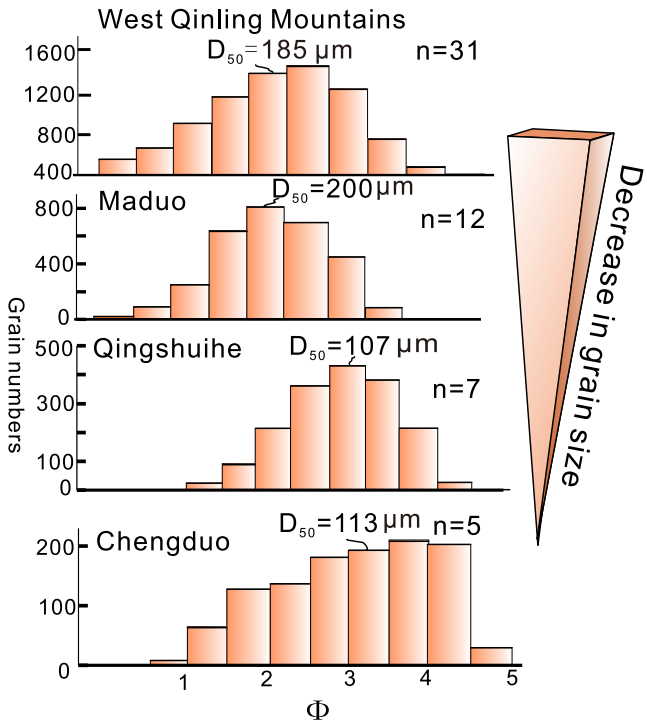

Figure 5. Grain-size distribution for the studied Triassic sandstones. D50: 50th percentile (median particle size). n = Number of samples; $\Phi = -\log_2 D$; D = Grain diameter in millimeters (mm).

In the Diebu and Lazikou sections, the lower part of the unit mostly consists of massive and bioclastic shallow-marine limestone. In the middle part of the Diebu section, a fault separates calcareous sandstones and shallow-marine limestones (Figure 4g). The upper part is dominated by calcareous sandstones with sole marks and incomplete Bouma sequences interbedded with mudrocks, indicating a bathyal-abyssal environment. The same up-section transition to interbedded sandstones and mudrocks with distinct turbiditic characteristics is displayed in the Lazikou section.

4.1.4. Bayankhara Group

The Bayankhara Group in the central Songpan-Ganzi basin mostly consists of interbedded sandstone and mudrock (Figure 4i). More abundant carbonate interlayers in the lower part pass gradually up-section to dominant siliciclastic sediments. Incomplete Bouma sequences and soft-sediment deformation structures are observed throughout the section (Figure 4j). Deposition in submarine channels, fan lobes, and fan fringe/hemipelagic settings is indicated.

4.2. Sandstone Petrography and Heavy Minerals

The median size D_{50} of the studied sandstones from the West Qinling Mountains is 185 μm. In the Bayankhara Group, sandstones are notably coarser in the Maduo area (D_{50} 200 μm) than in the Qingshuihe (D_{50} 107 μm) and Chenduo areas (D_{50} 113 μm) (Figure 5).

Twelve sandstone samples from the Lower Carboniferous Badu Fm. are mostly feldspatho-litho-quartzose (average $Q_{59}F_{15}L_{26}$) (Figure 6a), with volcanic (37%–72%) and low-rank metamorphic lithics (20%–60%) (Figure 7). Twenty-six sandstone samples from the Maomaolong Fm. are similarly feldspatho-litho-quartzose (average Q_{58} F_{14} L_{28}) (Figures 6c and 6d), documenting an up-section increase of sedimentary lithic fragments from 1% to 50% (Figure 7). Sixteen sandstone samples from the Longwuhe Fm. are mainly litho-quartzo-feldspathic (average $Q_{42}F_{46}L_{12}$) (Figures 6e and 7), with mostly volcanic and metamorphic lithics (Figure 6e). Ten sandstone samples from the Gulangdi Fm. are richer in lithic fragments (20%) than the underlying unit.

Twenty-four sandstone samples from the Bayankhara Group are mostly litho-feldspatho-quartzose (average $Q_{50}F_{27}L_{23}$), with volcanic (31%–64%), metamorphic (22%–57%), and minor sedimentary lithics (5%–25%) (Figure 6f).

From the Badu Fm. to the Gulangdi Fm., the ratio between sedimentary and volcanic lithics first increases and then decreases up-section. The quartz/feldspar ratio is higher in Triassic sandstones of the Bayankhara area (Figure 7).

Heavy minerals in Maomaolong Fm. sandstones are mostly zircon, tourmaline, and rutile (Figure 8), the sum of their percentages (ZTR index) varying from 68 to 92 (Table S2). Sandstones of the Longwuhe Fm. and Gulangdi Fm. show an increase in epidote (5%–15% vs. 0%–5%) and garnet (3%–11% vs. 0%–2%) in the West Qinling Mountains (ZTR 22–34), whereas zircon, apatite, and tourmaline characterize the Bayankhara Group (ZTR 51–81) (Figure 8).

4.3. U-Pb Zircon Geochronology

The three porphyry granites dated from the Hezuo section yielded ages of 238.0 ± 0.7 Ma (MSWD = 1.8; 23WQL165) and 233.6 ± 0.5 Ma (MSWD = 6.923; 23WQL183) for those intruding the lower Maomaolong Fm., and of 244.8 ± 2.1 Ma (MSWD = 2.6; 23WQL62) for the one intruding the upper Maomaolong Fm. (Figure 9).

Detrital zircons in sandstone sample 23WQL81 from the Badu Fm. in the Yangsha area display major age peaks at 445 and 937 Ma, and minor clusters at ~1,420 and ~2,390 Ma (Figure 10).

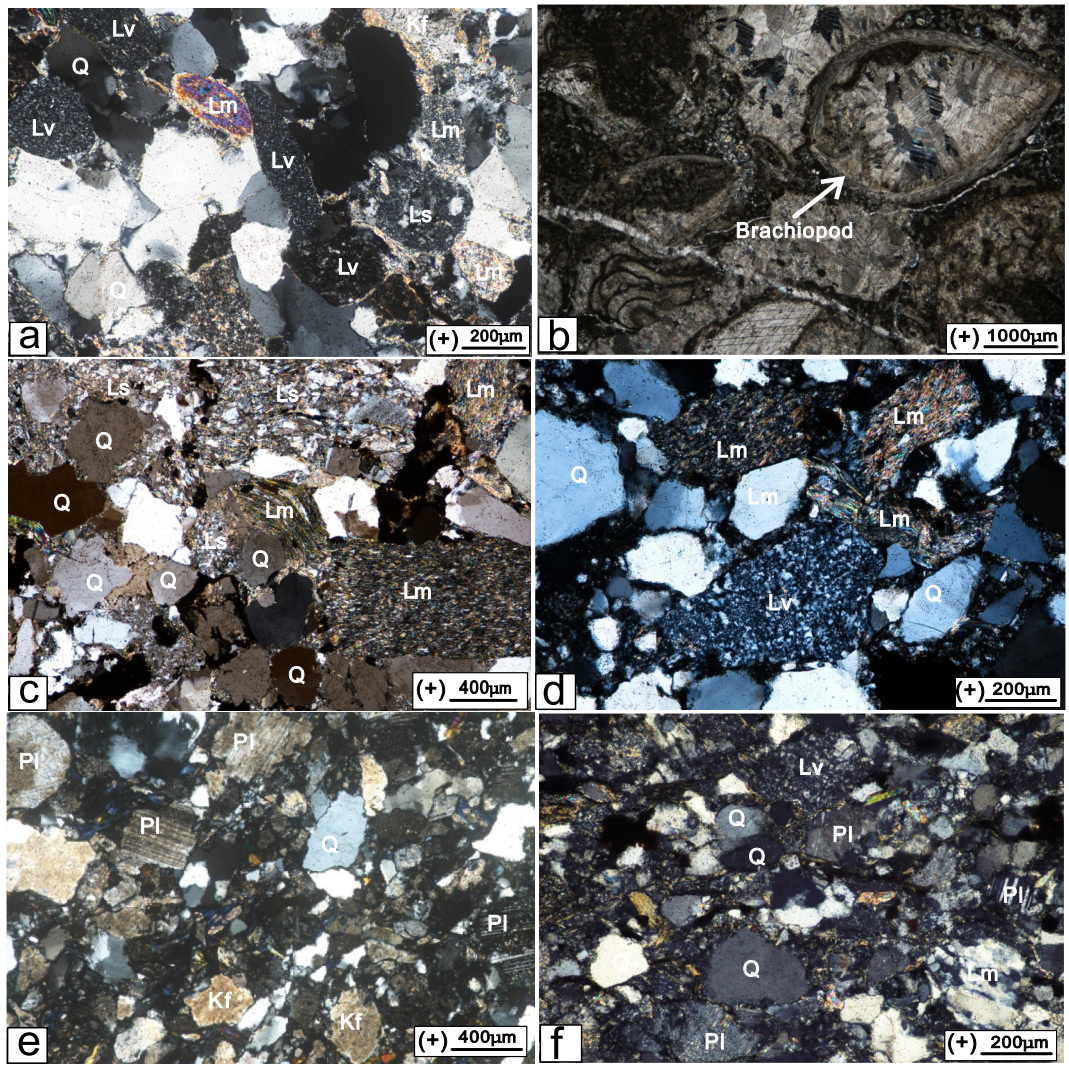

Figure 6. Photomicrographs under crossed polars: (a) litho-quartzose sandstone (23WQL86; Badu Fm., Yangsha area); (b) brachiopod in slumped limestone (Maomaolong Fm., Longwuhe section); (c) litho-quartzose sandstone (23WQL39; Maomaolong Fm., Madang section); (d) litho-quartzose sandstone (23WQL175; Maomaolong Fm., Hezuo section); (e) quartzo-feldspathic sandstone (23WQL306; Longwuhe Fm., Longwuhe section); (f) feldspatho-litho-quartzose sandstone (22GD10; Bayankhara Group). Q = quartz (Monocrystalline quartz, Polycrystalline quartz); Pl = Plagioclase feldspar, Kf = Potassium feldspar; Lv = volcanic fragment; Ls = sedimentary fragment, Lm: metamorphic fragment.

Ten sandstones from the Maomaolong Fm. (Figure 10) can be subdivided into two groups. Group 1 samples 24WQL24, 24WQL42, 23WQL49, 23WQL155, 23WQL166, 23WQL175, and 23WQL195 are characterized by a main peak at 456–457 Ma and minor Neoproterozoic ages. Group 2 samples 23WQL55, 23WQL63, and 23WQL68 are characterized by a main peak at 1,906–1,928 Ma and minor clusters at 2,283–2,300 Ma and 302–341 Ma. The youngest single-grain age obtained from the Hezuo section is 262.0 ± 1.2 Ma (23WQL68). A pebble from the Maomaolong Fm. in the Madang section yielded peaks at 440 Ma and 823 Ma, consistent with those obtained from the Badu Fm. (Figure 10).

4.4. Depositional Ages

The youngest U-Pb ages of detrital zircons from the Maomaolong Fm. are 252.0 ± 2.0 Ma (n = 2) and 255.7 ± 1.2 Ma (n = 2), whereas the ages of the oldest igneous rocks intruding the Maomaolong Fm. are 246.0 ± 1.0 Ma (n = 2) and 246.0 ± 2.0 Ma. Considering the superimposition relationship with the overlying Longwuhe Formation, these data tightly constrain the depositional age as older than 250 Ma and younger than 256 Ma (i.e., Late

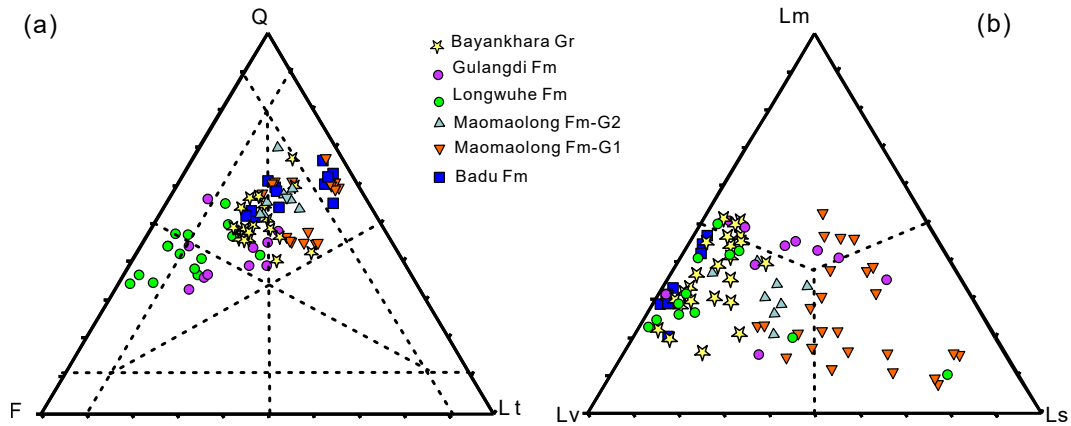

Figure 7. Sandstone petrography in West Qinling Mountains and Bayankhara area: (a) Q-F-L plot (compositional fields from Garzanti, 2019); (b) Lm-Ls-Lv plot.

Permian-earliest Early Triassic). The presence of Late Carboniferous to Early–Middle Permian fusulinids (*Schwagerina* sp. and *Parafusulina* sp.), brachiopods (*Uncinunellina* cf. *wangenheimi* (Pander); BGMRGS, 1989), corals, and gastropods in limestone clasts further indicates deposition after the Middle Permian (L. Li et al., 2014).

The youngest detrital zircons from the overlying Longwuhe Fm. are dated as 249.1 ± 1.4 Ma (n = 5) and 249.5 ± 0.5 Ma (n = 38; Table S7; Figure 11), whereas the oldest intrusive rocks in the West Qinling Mountains are dated as 246.0 ± 1.0 Ma and 244.4 ± 2.0 Ma (Figure 11). The indicated depositional age between 250 and 246 Ma (around the Early/Middle Triassic boundary) for the Longwuhe Fm. in the study area is consistent with the abundant Early/Middle Triassic bivalves and ammonites, including *Claraia bittner*, *Meekoceras* sp., and *Columbites* sp. (BGMRGS, 1989; Yin, 1992).

The youngest detrital zircons from the overlying Gulangdi Fm. are dated as 243.0 ± 3.3 Ma (n = 2), 244.4 ± 1.8 Ma (n = 3) and 245.0 ± 7.3 Ma (n = 2; Table S7; Figure 11), whereas the oldest intrusive rocks are dated as 242.3 ± 2.8 Ma and 242.0 ± 2.6 Ma. Deposition in the Anisian (245–242 Ma; early Middle Triassic; Figure 11) is supported by ammonites and nautiloids including *Hollandites* sp., *Hollandites* cf. *voiti*, *Enoploceras* sp., and *Trematoceras* sp. (BGMRGS, 1989).

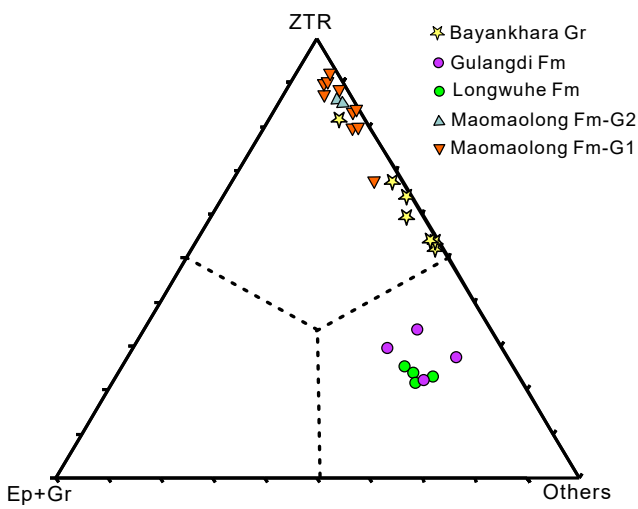

Figure 8. Heavy minerals in sandstones from West Qinling Mountains and Bayankhara area. Ep: epidote; Gr: garnet; ZTR: zircon + tourmaline + rutile; Others: other transparent heavy minerals.

The youngest detrital zircons from the Bayankhara Group in the Songpan-Ganzi basin are dated as 240.9 ± 1.2 Ma (n = 8), 241.2 ± 2.3 Ma (n = 5) and 241.8 ± 2.6 Ma (n = 7; Figure 11; Table S7) and the oldest intrusive rocks as 228.4 ± 1.9 Ma and 225.0 ± 3 Ma, suggesting an inferred depositional interval of approximately 242–228 Ma (late Middle–early Late Triassic) (Table S7).

5. Discussion

5.1. Paleogeographic Evolution

From the Carboniferous Badu Fm. to the Lower-Middle Permian Daguanshan Fm., the sedimentary succession of the West Qinling Mountains documents a monotonous alternation of shoal, platform-margin, and semi-restricted platform facies (Figures 3 and 14a; Gao, 2019; P. Li et al., 2025). Paleontological studies revealed that the fusulinids *Profusulinella praetypica* and *P. isvarica* and the conodont *Neogondolella clarki* from Carboniferous strata of the Lixian area share a biogeographic affinity with the South China block (Guo, 2003). This suggests that North China and South China were not separated by an ocean at that time, and that the study area was a shallow-marine domain located somewhere between North China and South China.

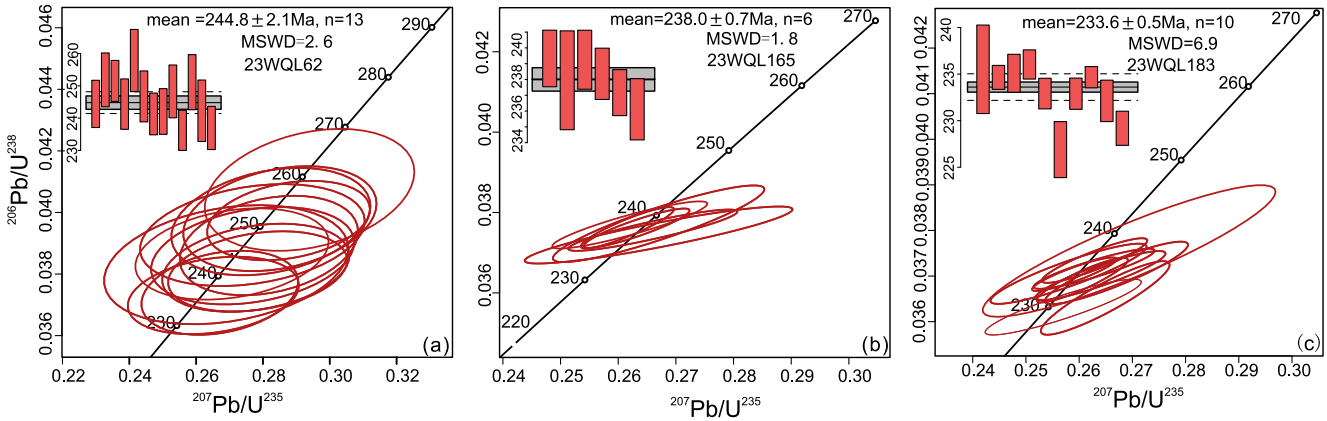

Figure 9. Zircon U-Pb Concordia diagrams with weighted mean $^{206}Pb/^{238}U$ ages (1σ uncertainties) for porphyry granites intruding the Maomaolong Fm. in Hezuo section. MSWD = mean square weighted deviation.

A clear north-to-south facies distribution is documented in the Early Triassic during deposition of the Maomaolong Fm., when continental-slope facies in the northern Longwuhe and Chaka areas passed southward to deep-marine turbidites in the Hezuo and Madang regions; shallow-marine carbonate facies persisted in the Diebu and Lazikou areas farther south (Figures 3, 14b, and 14c; Y. Z. Chen, 2013; Yin, 1992).

In the latest Early Triassic to early Middle Triassic (249–243 Ma), deep-sea turbidites of the Longwuhe and lower Gulangdi formations were deposited in both northern and central regions, with depocenter located in the Hezuo-

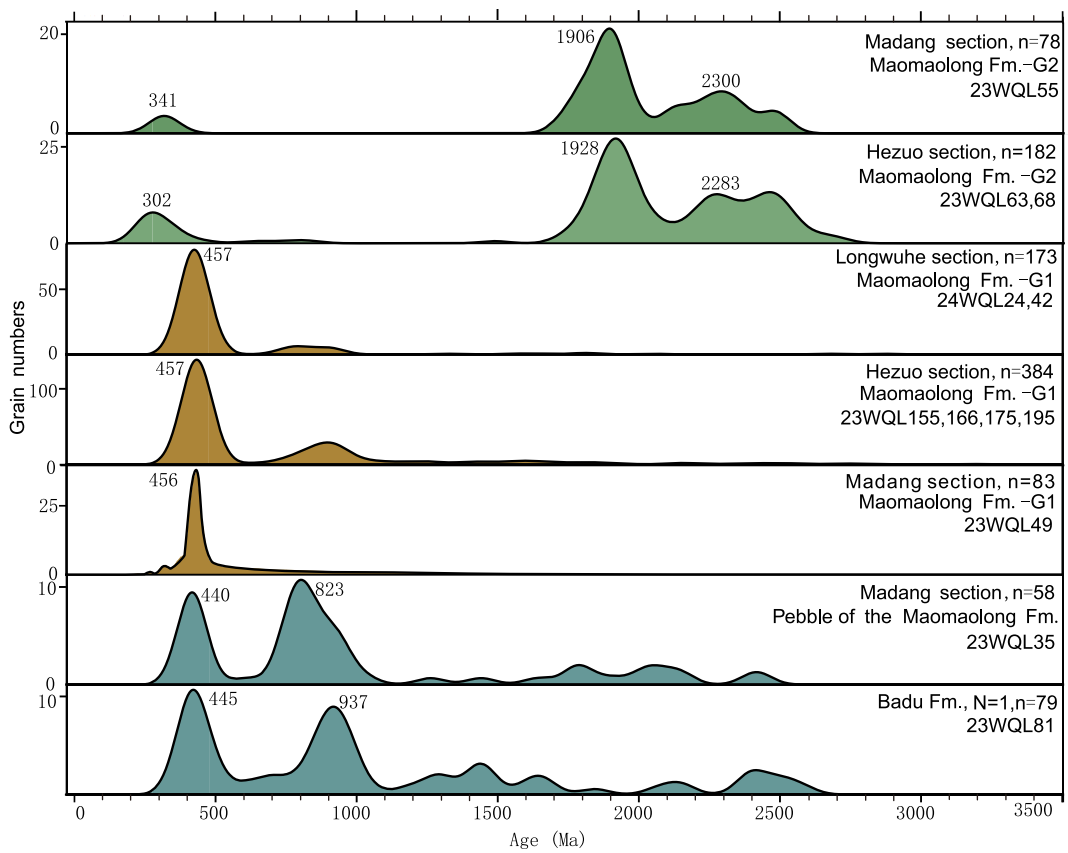

Figure 10. Kernel density estimates plots of analyzed zircon ages from Carboniferous-Triassic strata of the West Qinling Mountains. Bandwidth 30 Ma (50 Ma for histograms). *N*=Sample numbers; *n* = Grain numbers.

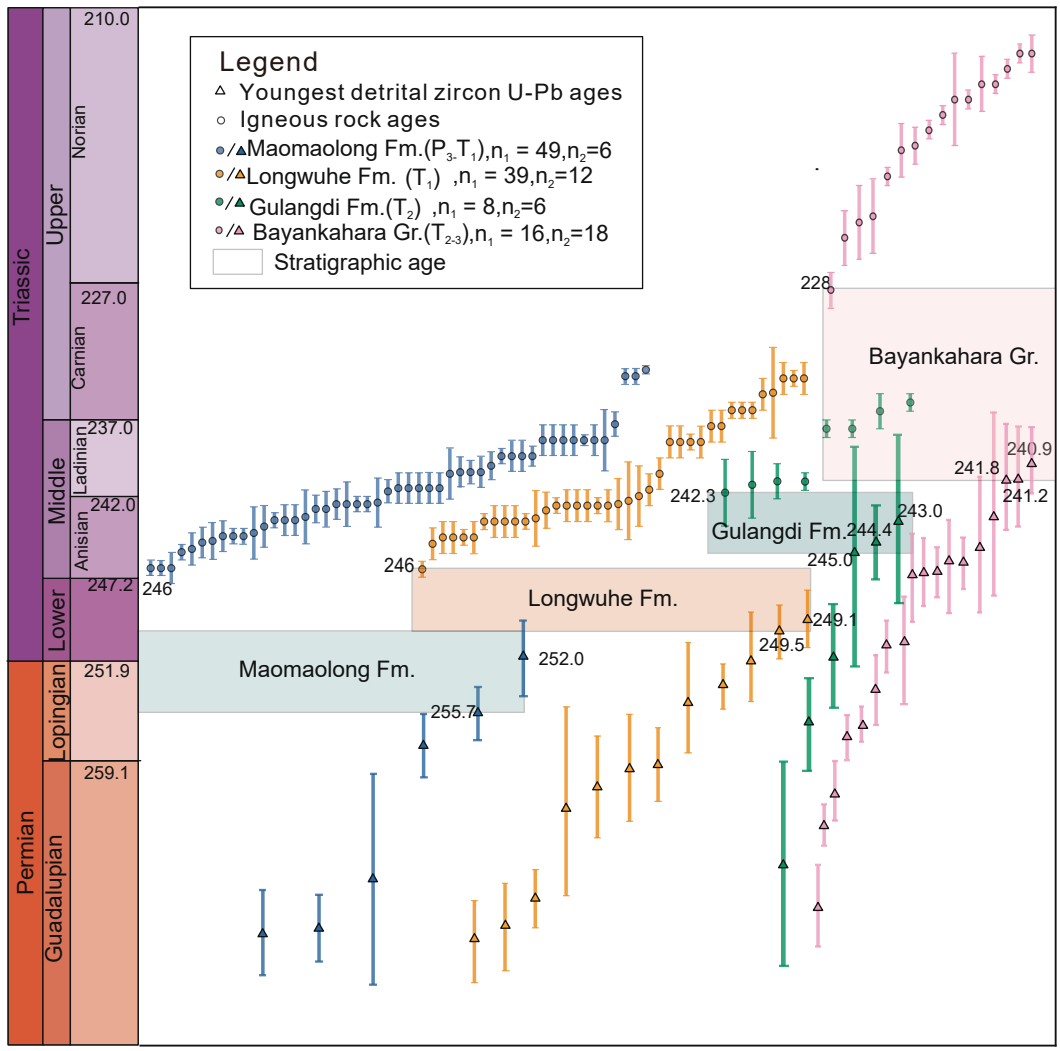

Figure 11. Stratigraphic age constrained by youngest ages of detrital zircons and oldest ages of intruded igneous rocks. The youngest detrital-zircon ages are given as Y1δ (2+) (weighted mean ages ±1σ, including both internal analytical error and external systematic error). $n1$ = Number of intruded igneous rocks, $n2$ = Number of samples used to calculate the youngest detrital-zircon ages.

Zhuoni area. The Diebu and Lazikou areas were still characterized by shallow-marine carbonates at that time (Figures 3 and 14d).

By the Middle Triassic (243–242 Ma), during deposition of the upper Gulangdi Fm., the depocenter migrated southward, and turbiditic sedimentation took place across the West Qinling Mountains, including the Diebu and Lazikou areas. Even the Bailongjiang highland (Yin, 1992), a southern paleo-uplift where platform carbonates accumulated since the Devonian (H. F. Yin & Peng, 1995), was drowned and started to receive siliciclastic detritus in the Ladinian (Bayankhara Group turbidites; Figures 3 and 14e; X. Li et al., 2012).

5.2. Provenance Interpretation

Zircons contained in the studied sandstones from the Carboniferous Badu Fm. yielded age peaks at 445 and 937 Ma, well comparable with zircon ages from the East Kunlun-Qilian-Qaidam terrane and Qinling orogenic belt (Figure 12). Published detrital-zircon data from Silurian-Carboniferous strata of the West Qinling Mountains (P. Li et al., 2025; Y. D. Pan & Hu, 2024; Y. X. Zhang et al., 2014) indicate similar age peaks, suggesting unchanged provenance through much of the Paleozoic (Figure 13). We infer that from Silurian to Carboniferous

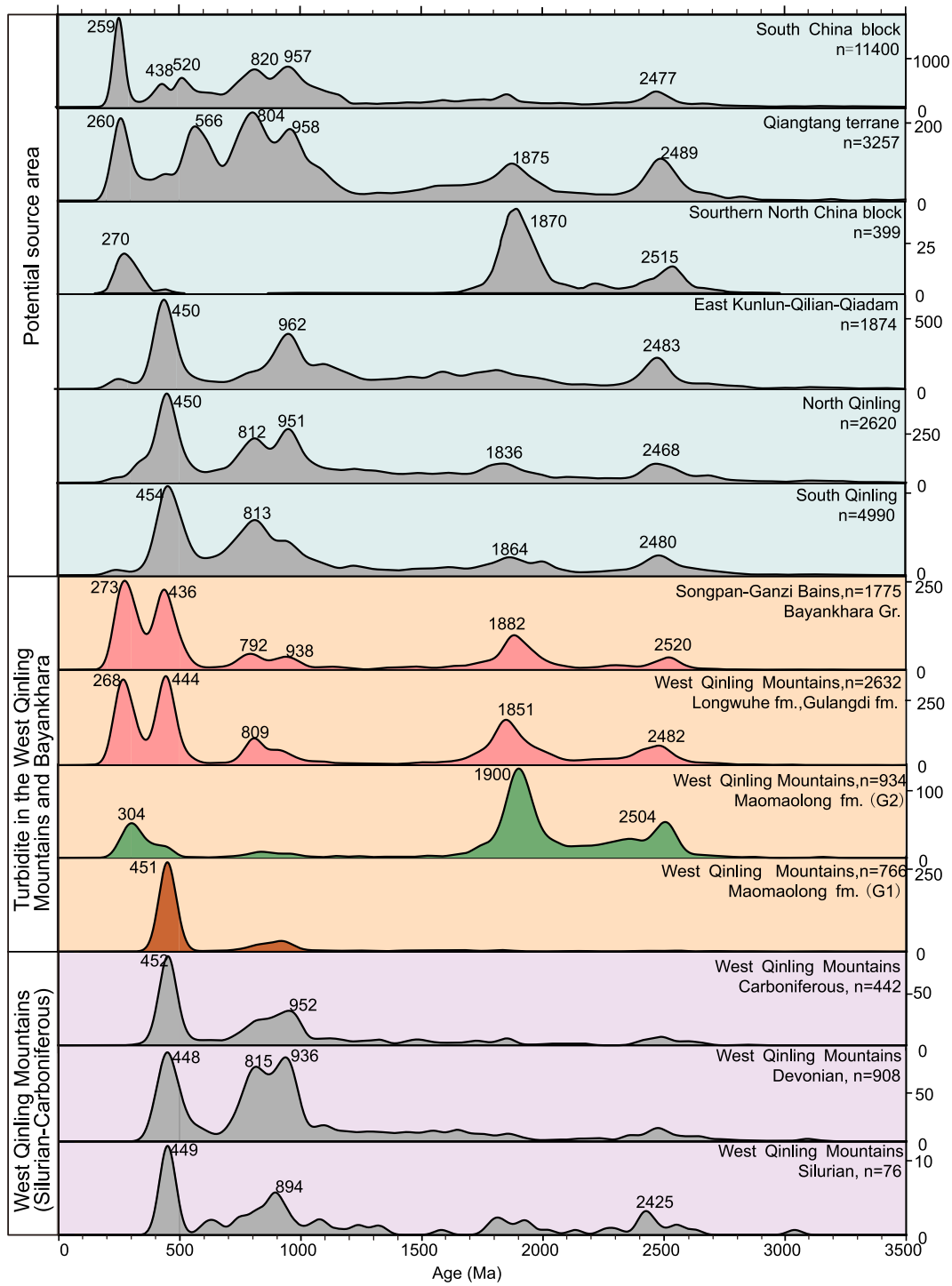

Figure 12. Kernel density estimates plots of U-Pb zircon ages characterizing potential source terranes. Data sources: X. Wang et al. (2018) and W. T. Yang et al. (2023); W. Yang et al. (2025) for southern North China block; Chai et al. (2024) for North and South Qinling belts (NQL and SQL); W. D. He et al. (2023) for East Kunlun-Qilian-Qaidam terranes; T. L. Xia et al. (2024) for the South China block; Tang et al. (2023) for Qiangtang block; Y. D. Pan and Hu (2024) for West Qinling Mountains (WQL) and Bayankhara Group (longitude between 95°E and 100°E; Table S6).

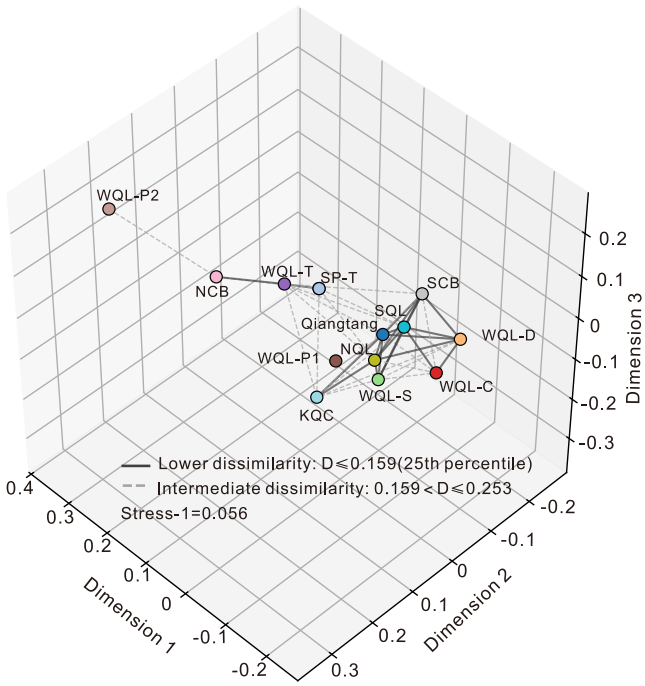

Figure 13. Three-dimensional multidimensional scaling (3D-MDS) plot illustrating the similarity of detrital zircon U-Pb age spectra in West Qinling Mountains (WQL-T: Triassic samples; WQL-C: Carboniferous samples; WQL-D: Devonian samples; WQL-S: Silurian samples) versus adjacent terranes (SCB: South China Block; NCB: North China Block; KQC:East Kunlun-Qaidam-Qilian terranes; SP-T: Triassic samples of the Songpan-Ganzi Basin).

times detritus from the South China block farther south could not bypass the extensive belt of shallow-marine sediments deposited in the southern part of the West Qinling Mountains.

In the Maomaolong Fm., Group 1 sandstones are characterized by abundant sedimentary rock fragments, durable heavy minerals, and similar detrital-zircon ages, suggesting extensive recycling of older strata (Figures 12 and 13). The same U-Pb age peaks at 440 and 823 Ma of zircons contained in the pebble collected in the Madang section from the Maomaolong Fm. support this interpretation (Figure 10). The abundance of limestone clasts, ooids and bioclasts testifies to major supply from shallow-water carbonates. The numerous carbonate-rich megabeds contained in this unit (P. Li et al., 2025) may have been derived from either side of the basin, since similar carbonate platforms exist both to the north and to the south. Most detritus of Group 1 sandstones was thus derived from intrabasinal recycling of Carboniferous to Lower Permian strata.

Detrital-zircon ages in Group 2 sandstones, instead, show a strong affinity with compiled ages from the southern margin of the North China block, as highlighted in the MDS plot (Figures 12 and 13; Darby & Gehrels, 2006; W. Yang et al., 2025). Qinling, East Kunlun-Qilian-Qaidam terranes, dominated by Neoproterozoic basement rocks with zircon ages mostly in the 750–1,000 Ma range, are instead ruled out as potential sources (Figure 12). Group 1 and 2 signatures were already identified in previous studies, which documented the prevalence of Group 1 in the eastern Xunhua, Jiangligou, and Hezuo areas, and of Group 2 in the eastern Lintan and Minxian regions (Jiang et al., 2025). Our new data, however, show that Group 2 sandstones widely occur also in the Longwuhe, Madang, and Hezuo areas, indicating that their distribution may have been temporally rather than spatially constrained (Figure 2b; L. Chang, 2019; Gao, 2019; Jiang et al., 2025; P. Li et al., 2025; H. C. Yu et al., 2022).

In the Longwuhe Fm., a marked increase in feldspars, felsic igneous rock fragments, and metamorphic heavy minerals indicates additional supply from magmatic and metamorphic rocks. This interpretation is supported by the appearance of additional Early Paleozoic (~420–480 Ma) and Neoproterozoic (~750–1,000 Ma) detrital-zircon age peaks (Figure 12). A comparative analysis among potential sources suggests that such detritus was derived from either the East Kunlun-Qilian-Qaidam terranes or/and Qinling orogenic belt, where magmatic and metamorphic rocks of these ages are widely exposed (Figures 12 and 13). Paleocurrent data indicate a persistent input of platform-carbonate detritus from the south (L. Li et al., 2014; P. Li et al., 2025).

The Gulangdi Fm. shares similar petrographic, heavy-mineral, and zircon-age signatures as the Longwuhe Fm., indicating unchanged provenance. A notable decrease in limestone gravel and dominant south-directed paleocurrents (Figure 3), however, indicate ceasing sediment supply from carbonate platforms in the south and primary detrital sources from the East Kunlun-Qilian-Qaidam terranes, Qinling orogenic belt, and North China block.

The Bayankhara Group exhibits similar detrital-zircon age peaks as Triassic strata of the West Qinling Mountains (Figures 12 and 13). Southward paleocurrents (Figure 2b) and a progressive southward decrease in grain size (Figure 5), together with the detrital-zircon age distributions, suggest that sediment was transported predominantly southward from the East Kunlun-Qilian-Qaidam terranes and Qinling orogenic belt (Figure 12). Although the Qiangtang block has been proposed as a potential source for the Bayankhara Group, its prominent Pan-African zircon-age signal is not evident in the available data sets from the central Songpan-Ganzi basin, suggesting that its contribution to this part of the basin was limited (Xue et al., 2023; Figure 12). Moreover, the central basin is dominated by zircon spectra with unimodal peak at ~243 Ma or bimodal Permian and ~430 Ma peaks, with only minor Neoproterozoic ages (data in Y. Liu et al., 2025). Considering that zircon-age spectra in the South China block are characterized by a major Neoproterozoic peak, and that carbonate platforms extensively developed along its western margin in the Early-Middle Triassic (Peng et al., 2021; Y. Wang et al., 2023), the South China block is also ruled out as a significant source.The available evidence thus suggests that the central Songpan-Ganzi

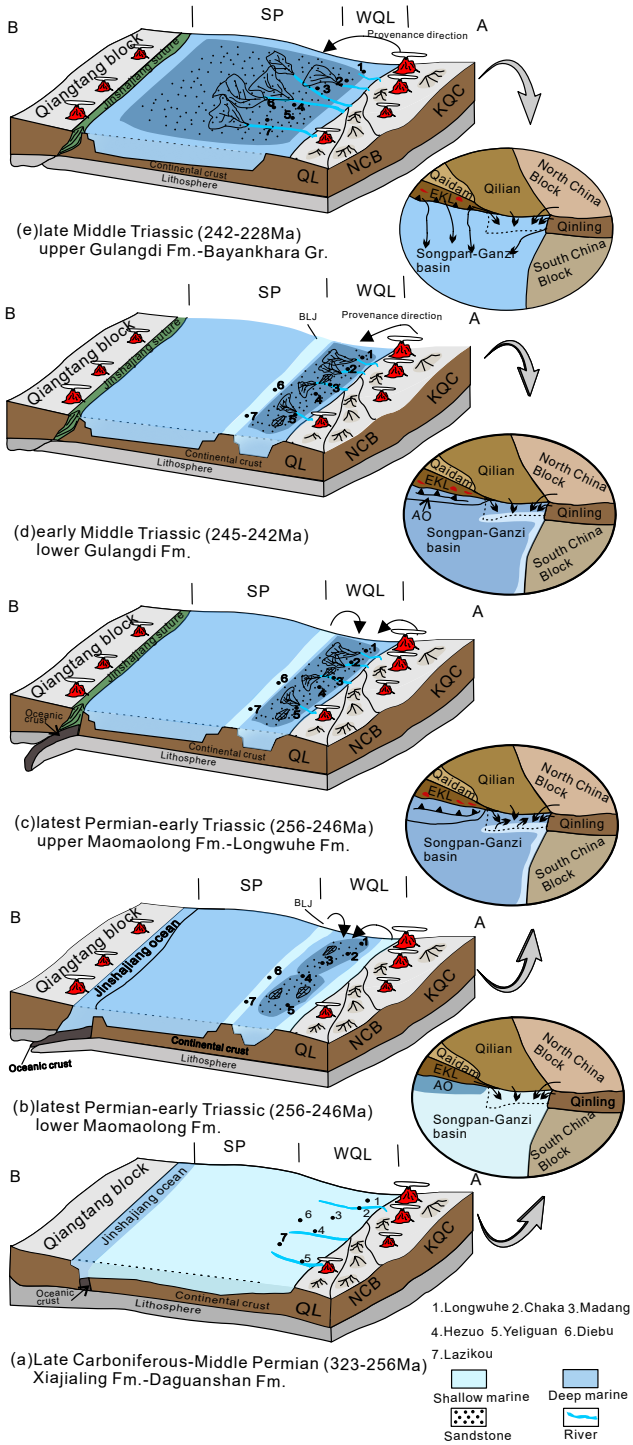

Figure 14.

basin received siliciclastic detritus primarily from the East Kunlun-Qilian-Qaidam terranes and the Qinling orogenic belt.

5.3. Testing the Remnant-Ocean-Basin Hypothesis

A most popular view is that the Songpan-Ganzi deep-sea turbidites accumulated in the remnant-ocean basin resulting from the collision between the South China and North China blocks. Several lines of evidence, however, contradict this model: (a) a remnant-ocean-basin succession should theoretically exhibit a shallowing and coarsening-upward trend, passing up-section from abyssal sediments (e.g., chert), to deep-sea flysch, and eventually molassic deltaic and fluvial sediments (Weislogel et al., 2006, 2010; Zhou & Graham, 1995). Field observations, however, document a quite opposite, deepening-upward trend from Lower Carboniferous shallow-marine deposits to Middle Triassic deep-sea turbidites (L. Li et al., 2014); (b) age spectra of detrital zircons do not support provenance from the Qinling-Dabie orogenic belt (L. Ding et al., 2013; Jian et al., 2019; Tang et al., 2023); (c) integrated provenance analysis indicates that Triassic Songpan-Ganzi turbidites were primarily sourced from the East Kunlun-Qilian-Qaidam terranes, Qinling orogenic belt, and North China block; (d) our samples do not contain the high-pressure metamorphic detritus expected if the Dabie orogen were a main source for Songpan-Ganzi turbidites (Figure 8; Avigad, 1995); (e) the northern West Qinling Mountains document platform-carbonate sedimentation from the Carboniferous to the Middle Permian, consistent with deposition on the southern passive continental margin of the North China block (F. Q. Yang & Wang, 1995); (f) last but not least, deep seismic reflection profiles show that the West Qinling Mountains are underlain by crystalline basement (H. Li et al., 2023; Mooney et al., 2005; H. Wang et al., 2014; K. J. Zhang, 2001).

5.4. The Hyper-Extended Continental Margin Hypothesis

The following pieces of evidence indicate that the Triassic Songpan-Ganzi turbidites exposed in the West Qinling Mountains were deposited on a hyper-extended continent-ocean transition rather than in a remnant ocean basin: (a) provenance analysis of the Maomaolong (Group 2 sandstones) and Longwuhe formations indicates that the northern West Qinling Mountains received a large amount of detritus from the carbonate platform in the south. The Gulangdi Fm. was instead fed by the East Kunlun-Qilian-Qaidam terranes and Qinling orogenic belt in the north, suggesting progressive basin

Figure 14. Envisaged tectono-sedimentary evolution of West Qinling Mountains (WQL) with corresponding paleogeographic maps. The cross sections follow the A–B transect shown in Figure 2; A and B denote the transect endpoints. Late Carboniferous-Middle Permian (a): sediment supply from East Kunlun-Qilian-Qaidam terranes and Qinling orogenic belt in the north; depocenter located along Xiahe-Lixian line in southern part of study area. Latest Permian (b): sediment largely recycled intrabasinally from older strata; further basin expansion. Latest Permian-Early Triassic (c): sediment sourced from both East Kunlun-Qilian-Qaidam terranes and North China block in the north and carbonate platforms in the south; older strata completely eroded. Early Middle Triassic (d): sediment derived only from East Kunlun-Qilian-Qaidam terranes and North China block in the north; continuing basin expansion. Late Middle Triassic (e): entire Songpan-Ganzi basin receives sediment from East Kunlun-Qilian-Qaidam terranes and North China block in the north after southward migration of depocenter. BLJ: Bailongjiang uplift; KQC: East Kunlun-Qilian-Qaidam terranes; NCB: North China block; SP: Songpan-Ganzi basin; AO: A'nyemaqen Ocean; QL:Qinling.

expansion at the expense of southern shallow-water areas; (b) paleocurrents indicate both southward and northward flow in the Longwuhe Fm., but exclusively southward flow in the Gulangdi Fm., consistently with basin expansion and drowning of southern shallow-water areas (Figure 2b; Jian et al., 2019; L. Li et al., 2014; P. Li et al., 2025; Weislogel et al., 2010); (c) the deepening-upward sedimentary evolution from shoal, platform-margin, and semi-restricted platform facies in the Early Carboniferous to deep-sea turbidites in the Triassic is consistent with an extensional continental basin; (d) the occurrence of gabbro and diabase in the Longwuhe area is consistent with rifting active at Late Permian to early Middle Triassic times (L. Li et al., 2014); (e) lithofacies characteristics, geochemical features, and compositional signatures of Carboniferous to Middle Triassic sedimentary rocks in the northern West Qinling Mountains compare well with those of the South Qilian terrane (Y. Z. Chen, 2013).

The available evidence supports an extensional continental-margin interpretation for the studied succession. The dynamic mechanism of tectonic extension, however, still needs to be clarified. L. Li et al. (2014) proposed that the extension in the West Qinling Mountains resulted from slab rollback of the Yidun arc. Recent studies, however, have demonstrated that the magmatic rocks in the Yidun terrane formed in a syn- to post-collisional setting rather than in a subduction-related island arc (X. Hu et al., 2026), challenging the back-arc extension model. Given the uncertainties surrounding the back-arc extension model, an alternative tectonic framework is required to explain the Triassic hyper-extension event documented in the Songpan-Ganzi Basin and the West Qinling Mountains. The exact cause of such large-scale crustal extension remains unclear. Several authors have hypothesized that major changes in plate motion and boundary networks could induce far-field stress perturbations, leading to intracontinental extension far from active plate margins (Coblentz et al., 1998; Raimondo et al., 2014; Silva et al., 2018); Zheng et al. (2025) hypothesized that the Cenozoic India-Eurasia convergence might have been driven by slab pull from the Sumatra-Java subduction zone thousands of kilometers away, rather than by the push force from the Himalayan collision zone. Qian and Wang (2025) speculated that the Yanshanian event in East Asia—characterized by episodic intracontinental contraction and extension—was caused by global plate reorganizations during Pangea breakup, with interplate forces transmitted thousands of kilometers inland to induce large-scale extension. From this perspective, far-field stresses associated with global or regional plate reorganization may have contributed to the inferred Late Permian–Middle Triassic extension in the Songpan-Ganzi Basin. Alternatively, S. N. Liu and Wang (2023) envisaged an intracontinental rift system associated with the Emeishan mantle plume in the Danba-Xiaojin area of the eastern Songpan-Ganzi basin. The carbonate breccias, mafic rocks, and deepening-upward sedimentary succession of the West Qinling Mountains can be interpreted as related to the same rift system, suggesting that the influence of the Emeishan mantle plume may have extended northward into this region.

The proposed tectono-sedimentary evolution of the West Qinling Mountains from the Carboniferous to the Middle Triassic is illustrated in Figure 14. Carboniferous to Triassic strata were deposited on the passive continental margin of the North China block undergoing progressive tectonic extension. Until the Middle Permian, the study area was dominated by shallow-marine carbonates, with subordinate siliciclastic sediment derived from the northern East Kunlun-Qilian-Qaidam terranes and Qinling orogenic belt (Figure 14a; Y. Z. Chen, 2013). Carboniferous–Permian shallow-marine platform carbonates and associated collapse breccias observed during our fieldwork in the Danba–Xiaojin area indicate local preservation of older sedimentary cover (see also S. N. Liu & Wang, 2023). The limited exposure of Carboniferous–Early Triassic strata in the central Songpan-Ganzi basin may reflect burial beneath the thick Triassic succession and subsequent tectonic modification, although their subsurface distribution and continuity remain uncertain.

In the latest Permian, carbonate breccias and conglomerates of the lower Maomaolong Fm. marked the end of carbonate-platform deposition in the study area. Coarse detritus eroded from actively uplifting rift shoulders, exposing crystalline basement and mostly limestone cover strata, was rapidly deposited as gravity flows (Figure 14b; BGMRGS, 1989; Cao et al., 1995; F. Q. Yang & Wang, 1995). Throughout the Early Triassic (upper Maomaolong and Longwuhe formations), erosion of northern uplifts in the East Kunlun-Qilian-Qaidam terranes and North China block generated volumes of detritus transferred southward into the Songpan-Ganzi basin and mixed with minor supply from carbonate platforms in the south (Figure 14c). The presence of gabbro and diabase bodies indicates that an E/W-trending rift basin formed in the Late Permian, evolving into a deep-water hyper-extended rift setting during the Early Triassic, as supported by the emplacement of mafic intrusions into the uppermost Lower to lowermost Middle Triassic Longwuhe Formation (L. Li et al., 2014). During the early Middle Triassic (Anisian lower Gulangdi Fm.), the basin continued to expand, fed by detritus from the northeast

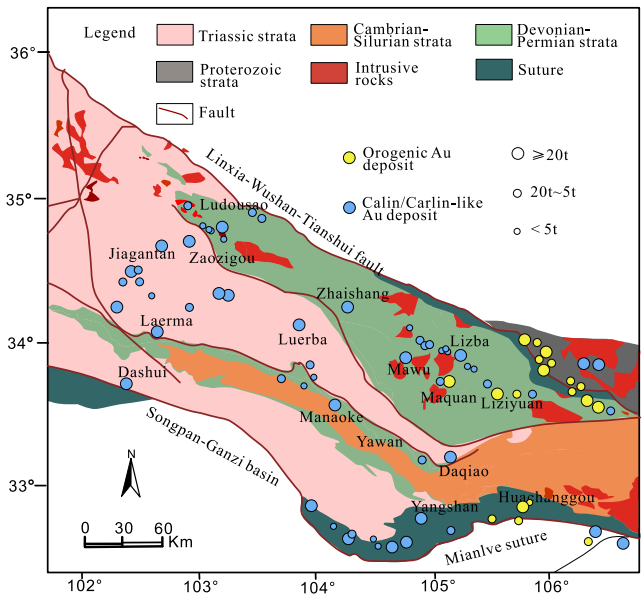

Figure 15. Ore deposits of the West Qinling Mountains (mod. after J. He et al., 2024).

Kunlun-Qilian-Qaidam terranes and North China block in the northeast (Figure 14d). During the late Anisian (upper Gulangdi Fm.), tectonic extension propagated southward to reach the Diebu area, where carbonate debris flows and siliciclastic turbidites of the Bayankhara Group started to be deposited (Yin, 1992). Sediment supply was still from the northern East Kunlun-Qilian-Qaidam terranes and North China block, largely including detritus from Lower Paleozoic magmatic rocks (Figure 14e).

6. Implications

This study shows that turbidites of the West Qinling Mountains and Bayankhara Group share the same provenance, implying that the Animaqing Ocean closed by ~243 Ma. This inference aligns with the widespread distribution of 240–220 Ma syn-collisional to post-collisional magmatic rocks in the East Kunlun orogenic belt (Z. Pan et al., 2022; S. G. Song et al., 2015; R. Xia et al., 2014).

The hyper-extended continental-margin scenario proposed in this study for the Songpan-Ganzi basin requires to profoundly reassess the tectonic affinity of Triassic magmatic rocks in the West Qinling Mountains. Within the proposed extensional continental-margin framework, a subduction-related arc origin for these magmatic rocks warrants reassessment, and a post-collisional origin may be considered, consistent with interpretations proposed for adjacent orogenic regions (e.g., X. Hu et al., 2026).

The West Qinling Mountains, as China's second-largest gold metallogenic province, hosts gold mineralization predominantly concentrated in the Late Triassic (Figure 15; 220–200 Ma; C. G. He et al., 2023; X. Yu et al., 2024). The traditional remnant-ocean-basin model implies a confined tectonic setting unfavorable for the generation of the large-scale hydrothermal fluid system required for extensive gold mineralization. This study, instead, argues that the West Qinling Mountains during the Carboniferous to Middle Triassic were the hyper-extended southern continental margin of the North China block. An extensional tectonic setting may have provided conditions favorable for Carlin-type gold mineralization, as proposed for the Nevada province in North America (Muntean et al., 2011). Lithospheric extension does not only generate the required heat source driving large-scale fluid circulation, but also creates a network of high-angle normal faults that provide crucial fluid pathways and ore-hosting structures. Consequently, the regional gold mineralization event that occurred in the West Qinling Mountains between 220 and 200 Ma is considered as a late-stage mineralization event, whereas an earlier mineralization event occurred during the basin-extension stage (Carboniferous to Middle Triassic) (J. J. Liu et al., 2019).

7. Conclusions

Through detailed stratigraphic investigations and turbidite provenance analyses conducted in the West Qinling Mountains, this study challenges the traditional remnant-ocean-basin model for Triassic Songpan–Ganzi turbidites, and supports the alternative hyper-extensional continental-margin model. The main conclusions are as follows:

1. the sedimentary succession exposed in the West Qinling Mountains documents progressive deepening environments from alternating shoal, platform-margin, and semi-restricted platform facies in the Early Carboniferous to deep-sea turbidites in the Middle Triassic;
2. Triassic turbidites were derived from the East Kunlun-Qilian-Qaidam terranes, North China block, and Qinling orogenic belt in the north, with undetected contribution from the Dabie orogenic belt;
3. Triassic turbidites of the Songpan-Ganzi basin were deposited on the hyper-extended continental margin of the North China block rather than in a remnant ocean basin;
4. An extensional tectonic setting may have provided favorable conditions for the formation of the region's world-class Late Triassic Carlin-type gold deposits.

Despite the sedimentological and geochronological constraints presented here, two key aspects warrant further investigation. First, detrital-zircon and heavy-mineral data identify source terrains but do not fully resolve sediment pathways and recycling processes. Future work should incorporate complementary single-grain techniques (e.g., geochemistry of detrital rutile, garnet, or spinel) to trace specific source rocks and evaluate the potential role of intermediate sedimentary storage, which may help explain the lack of Dabie-derived signals. Second, the enormous volume of Triassic turbidites in the Songpan–Ganzi basin (~2.0×10^6 km^3 deposited between ~250 and 228 Ma) documents one of the most dramatic episodes of continental erosion in the Earth's history. The associated large-scale silicate weathering and organic carbon burial plausibly contributed to a significant drawdown of atmospheric CO_2, potentially assisting in global climatic cooling and environmental stabilization after the end-Permian mass extinction.

Conflict of Interest

The authors declare no conflicts of interest relevant to this study.

Availability Statement

The data set (Y. Pan, 2026) supporting this research is provided as Supporting Information also available at https://figshare.com/s/50392218327f6b2b9df4.

Acknowledgments
We greatly appreciated the constructive comments and suggestions provided by the reviewers, Lin Li and one anonymous reviewer as well as the editorial handling by the editors, Djordje Grujic and Devon A. Orme. This study was supported by the Project of Deep Earth Exploration and Mineral Resource Prospecting, National Science and Technology Major Project of China (2024ZD1001103), and National Natural Science Foundation of China–Tethyan Project (Grant 91755209). We are grateful to Feiyue Chu, Dingjun Wen, and Xicuo Zha for their assistance in the field, and to Ben Kneller for constructive suggestions.

References

Avigad, D. (1995). Exhumation of the Dabie Shan ultra-high-pressure rocks and accumulation of the Songpan-Ganzi flysch sequence, central China: Comment. *Geology*, *23*(8), 764–765. https://doi.org/10.1130/0091-7613(1995)023<0764:EOTDSU>2.3.CO;2

BGMRGS (Bureau of Geology and Mineral Resources of Gansu Province). (1989). *Regional geology of Gansu province*. Geological Publishing House.

Bouma, A. H. (1964). *Turbidites[M]//Developments in sedimentology* (Vol. 3, pp. 247–256). Elsevier. https://doi.org/10.1016/S0070-4571(08)70967-1

Burchfiel, B. C., Zhiliang, C., Yupinc, L., & Royden, L. H. (1995). Tectonics of the Longmen Shan and adjacent regions, central China. *International Geology Review*, *37*(8), 661–735. https://doi.org/10.1080/00206819509465424

Cao, X. D., Zhao, J. T., & Hu, Y. X. (1995). Carboniferous paleogeographic characteristics and paleo-oceanic reconstruction in Qinling Mountains. *Earth Science–ournal of China University of Geosciences*, *20*(6), 624–630.

Chai, R., Yang, J. H., Deng, T., & Hu, X. M. (2024). A detrital zircon dataset for the eastern Central China Orogenic Belt (East Qinling, Dabie and Sulu orogens). *Geoscience Data Journal*, gdj3.232. https://doi.org/10.1002/gdj3.232

Chang, E. Z. (2000). Geology and tectonics of the Songpan-Ganzi fold belt, southwestern China. *International Geology Review*, *42*(9), 813–831. https://doi.org/10.1080/00206810009465113

Chang, L. (2019). Lithostratigraphic characteristics and chronostratigraphic discussion of the Middle-Lower Permian Shilidun formation in the Minxian area, West Qinling. *Chang'an University*.

Chen, B. W., Wang, K. Y., Liu, W. X., Cai, Z. J., Zhang, Q. W., Peng, X., et al. (1987). *Geotectonics of the Nujiang–Lancangjiang–Jinshajiang Region*. Geological Publishing House.

Chen, Y. Z. (2013). *A comparative study of tectonic and sedimentary characteristics between the South Qilian area and the north belt of the West Qinling Mountains*. Northwest University.

Cheng, H., & Cao, D. (2015). Protracted garnet growth in high-P eclogite: Constraints from multiple geochronology and P–T pseudosection. *Journal of Metamorphic Geology*, *33*(6), 613–632. https://doi.org/10.1111/jmg.12136

Coblentz, D. D., Zhou, S., Hillis, R. R., Richardson, R. M., & Sandiford, M. (1998). Topography, boundary forces, and the Indo-Australian intraplate stress field. *Journal of Geophysical Research*, *103*(B1), 919–931. https://doi.org/10.1029/97JB02381

Coutts, D. S., Matthews, W. A., & Hubbard, S. M. (2019). Assessment of widely used methods to derive depositional ages from detrital zircon populations. *Geoscience Frontiers*, *10*(4), 1421–1435. https://doi.org/10.1016/j.gsf.2018.11.002

Cronin, B. T. (2018). Lithofabric classification and distribution of coarse-grained deep-water clastic depositional systems. In C. C. Turner, & B. T. Cronin (Eds.), *Rift-related coarse-grained submarine fan reservoirs; the Brae Play, South Viking Graben, North Sea* (AAPG Memoir 115, pp. 39–96). American Association of Petroleum Geologists. https://doi.org/10.1306/13652178M1153311

Darby, B., & Gehrels, G. (2006). Detrital zircon reference for the North China Block. *Journal of Asian Earth Sciences*, *26*(6), 637–648. https://doi.org/10.1016/j.jseaes.2004.12.005

Deng, T., Hu, X., Chew, D., Wang, Q., Yu, J. H., & Drakou, F. (2024). Sedimentological evidence for pre-early Permian continental subduction in the Dabie orogen, central-east China. *Tectonics*, *43*(1), e2023TC007839. https://doi.org/10.1029/2023TC007839

De Sigoyer, J., Vanderhaeghe, O., Duchene, S., & Billerot, A. (2014). Generation and emplacement of Triassic granitoids within the Songpan Ganze accretionary-orogenic wedge in a context of slab retreat accommodated by tear faulting, Eastern Tibetan plateau, China. *Journal of Asian Earth Sciences*, *88*, 192–216. https://doi.org/10.1016/j.jseaes.2014.01.010

Dickinson, W. R., & Gehrels, G. E. (2009). Use of U–Pb ages of detrital zircons to infer maximum depositional ages of strata: A test against a Colorado Plateau Mesozoic database. *Earth and Planetary Science Letters*, *288*(1–2), 115–125. https://doi.org/10.1016/j.epsl.2009.09.013

Ding, L., Yang, D., Cai, F. L., Pullen, A., Kapp, P., Gehrels, G. E., et al. (2013). Provenance analysis of the Mesozoic Hoh-Xil-Songpan-Ganzi turbidites in northern Tibet: Implications for the tectonic evolution of the eastern Paleo-Tethys Ocean. *Tectonics*, *32*(1), 34–48. https://doi.org/10.1002/tect.20013

Ding, Q. F., Jiang, S. Y., & Sun, F. Y. (2014). Zircon U–Pb geochronology, geochemical and Sr–Nd–Hf isotopic compositions of the Triassic granite and diorite dikes from the Wulonggou mining area in the Eastern Kunlun Orogen, NW China: Petrogenesis and tectonic implications. *Lithos*, *205*, 266–283. https://doi.org/10.1016/j.lithos.2014.07.015

Dou, J., Siebel, W., He, J., & Chen, F. (2019). Different melting conditions and petrogenesis of peraluminous granites in western Qinling, China, and tectonic implications. *Lithos*, *336–337*, 97–111. https://doi.org/10.1016/j.lithos.2019.04.003

Enkelmann, E., Weislogel, A., Ratschbacher, L., Eide, E., Renno, A., & Wooden, J. (2007). How was the Triassic Songpan-Ganzi basin filled? A provenance study. *Tectonics*, *26*(4). https://doi.org/10.1029/2006TC002078

Feng, Y. M., Cao, X. D., & Zhang, E. B. (2002). *Process and dynamics of West Qinling Orogenic Belt*. Xi'an Map Press.

Feng, Y. M., Cao, X. D., Zhang, E. P., Hu, Y. X., Pan, X. P., Yang, J. L., et al. (2003). Evolution, tectonic pattern and properties of the West Qinling orogenic belt. *Northwestern Geology*, *36*(1), 1–10.

Gao, X. Y. (2019). Geological characteristics and significance of late Paleozoic sedimentary strata in Lintan area, West Qinling Mountains. *Chang'an University*.

Garzanti, E. (2019). Petrographic classification of sand and sandstone. *Earth-Science Reviews*, *192*, 545–563. https://doi.org/10.1016/j.earscirev.2018.12.014

Garzanti, E., & Andò, S. (2019). Heavy minerals for junior woodchucks. *Minerals*, *9*(3), 148. https://doi.org/10.3390/min9030148

Gehrels, G. E., Valencia, V. A., & Ruiz, J. (2008). Enhanced precision, accuracy, efficiency, and spatial resolution of U-Pb ages by laser ablation–multicollector–inductively coupled plasma–mass spectrometry. *Geochemistry, Geophysics, Geosystems*, *9*(3). https://doi.org/10.1029/2007GC001805

Guo, J. (2003). *Study on paleontology of Carboniferous strata in Lixian* [Master's thesis]. Chang'an University. (in Chinese).

Han, B. N., Jiang, Y. H., Liu, Y. C., & Zhang, M. (2024). Petrogenesis and tectonic implications of Triassic high-K calc-alkaline granitoids and mafic microgranular enclaves from the western West Qinling Orogen, Central China. *Lithos*, *482*, 107734. https://doi.org/10.1016/j.lithos.2024.107734

He, C. G., Li, J. W., Kontak, D. J., Jin, X. Y., Wu, Y. F., Hu, H., et al. (2023). An Early Cretaceous gold mineralization event in the Triassic West Qinling orogen revealed from U-Pb titanite dating of the Ma'anqiao gold deposit. *Science China Earth Sciences*, *66*(2), 316–333. https://doi.org/10.1007/s11430-022-1015-1

He, J., Ding, Z., Zhu, Y., Zheng, H. X., Zhang, W. R., & Liu, J. (2024). Metallogenic series and quantitative assessment of deposits in the western Qinling region, Gansu, China. *Earth Science Frontiers*, *31*(3), 218–234. https://doi.org/10.13745/j.esf.sf.2023.2.68

He, W. D., Sun, J. P., Dong, Y. P., Qian, T., Wang, T., He, L., & Qi, Y. K. (2023). A synthesis of available detrital zircon data from the Qilian-Qaidam-Kunlun collage, northern Tibet. *Geoscience Data Journal*, gdj3.225. https://doi.org/10.1002/gdj3.225

Hu, F. Y., Liu, S. W., Ducea, M. N., Chapman, J. B., Wu, F. Y., & Kusky, T. (2020). Early Mesozoic magmatism and tectonic evolution of the Qinling Orogen: Implications for oblique continental collision. *Gondwana Research*, *88*, 296–332. https://doi.org/10.1016/j.gr.2020.07.006

Hu, X., Wen, D., Pan, Y., Garzanti, E., Deng, T., Dong, X. L., et al. (2026). Syn-collisional origin of Yidun arc-like magmas and northern provenance of Songpan-Ganzi turbidites (eastern Tibet). *Terra Nova*, *38*(3), 149–162. https://doi.org/10.1111/ter.70025

Ingersoll, R. V., Bullard, T. F., Ford, R. L., Grimm, J. P., Pickle, J. D., & Sares, S. W. (1984). The effect of grain size on detrital modes: A test of the Gazzi-Dickinson point-counting method. *Journal of Sedimentary Research*, *54*(1), 103–116. https://doi.org/10.1306/212F83B9-2B24-11D7-8648000102C1865D

Jackson, S. E., Pearson, N. J., Griffin, W. L., & Belousova, E. A. (2004). The application of laser ablation-inductively coupled plasma-mass spectrometry to in situ U–Pb zircon geochronology. *Chemical Geology*, *211*(1–2), 47–69. https://doi.org/10.1016/j.chemgeo.2004.06.017

Jian, X., Weislogel, A., & Pullen, A. (2019). Triassic sedimentary filling and closure of the eastern paleo-Tethys Ocean: New insights from detrital zircon geochronology of Songpan-Ganzi, Yidun, and west qinling flysch in eastern Tibet. *Tectonics*, *38*(2), 767–787. https://doi.org/10.1029/2018TC005300

Jiang, Z., Meiduo, L., Li, Z., Zhang, Z., Li, X., Qin, X., et al. (2025). Provenance of middle-upper Permian sandstones in Lintan and Jiangligou areas, West Qinling, China: Insights from geochemistry, detrital Zircon chronology, and Hf isotopes. *Minerals*, *15*(10), 1024. https://doi.org/10.3390/min15101024

Jin, H. J., & Li, Y. C. (1995). Permian-triassic remains and their environmental significance in the West Qinling Mountains. *Geological science*, *30*(4), 321–328.

Kong, J. J., Niu, Y. L., Hu, Y., Zhang, Y., & Shao, F. L. (2020). Petrogenesis of the Triassic granitoids from the East Kunlun Orogenic Belt, NW China: Implications for continental crust growth from syn-collisional to post-collisional setting. *Lithos*, *364–365*, 105513. https://doi.org/10.1016/j.lithos.2020.105513

Kou, X. H., Zhang, K. X., Zhu, Y. H., Chen, Z. Q., Lin, Q. X., Chen, F. N., & Huang, J. (2009). Middle Permian seamount from Xiahe area, Gansu province, northwest China: Zircon U-Pb age, biostratigraphy and tectonic implications. *Journal of Earth Science*, *20*(2), 364–380. https://doi.org/10.1007/s12583-009-0030-3

Li, H., Gao, R., Huang, X. F., Wang, H. Y., Guo, X. Y., Liang, H. D., et al. (2023). Triassic convergence and tectonic evolution of the West Qinling orogen: Constraints from reflection-seismology imaging. *Gondwana Research*, *122*, 1–10. https://doi.org/10.1016/j.gr.2023.05.020

Li, L., Meng, Q. R., Pullen, A., Garzione, C. N., Wu, G., Wang, Y. L., et al. (2014). Late Permian–early Middle Triassic back-arc basin development in West Qinling, China. *Journal of Asian Earth Sciences*, *87*, 116–129. https://doi.org/10.1016/j.jseaes.2014.02.021

Li, P., Kneller, B., & Valdez Buso, V. (2025). Carbonate-rich megabeds within a Triassic siliciclastic deep-water system, West Qinling orogenic belt, Central China: Character, processes and implications. *Depositional Record*, *11*(1), 232–259. https://doi.org/10.1002/dep2.301

Li, R. B., Pei, X. Z., Li, Z. C., Liu, Z. Q., Chen, G. C., Chen, Y. X., et al. (2012). Geological characteristics of late Paleozoic-Mesozoic unconformities and their response to some significant tectonic events in eastern part of Eastern Kunlun. *Earth Science Frontiers*, *19*(5), 244–254.

Li, X., Wang, C., Liu, S., Ran, B., Xu, W. L., Zhou, Y., et al. (2012). Lithofacies of the Middle Triassic Guanggaishan Formation in the Bailongjiang uplift of Southwestern Qinling and its implications for Basin analysis. *Earth Science*, *37*(4), 679–692.

Li, X. W., Mo, X. X., Huang, X. L., Dong, G. C., Yu, X. H., Luo, M. F., & Liu, Y. (2015). U–Pb zircon geochronology, geochemical and Sr–Nd–Hf isotopic compositions of the Early Indosinian Tongren Pluton in West Qinling: Petrogenesis and geodynamic implications. *Journal of Asian Earth Sciences*, *97*, 38–50. https://doi.org/10.1016/j.jseaes.2014.10.017

Liu, H. N., Li, X. W., Mo, X. X., Xu, J. F., Liu, J. J., Dong, G. C., et al. (2021). Early Mesozoic crustal evolution in the NW segment of West Qinling, China: Evidence from diverse intermediate–felsic igneous rocks. *Lithos*, *396–397*, 106187. https://doi.org/10.1016/j.lithos.2021.106187

Liu, J. J., Liu, C. H., Wang, J. P., Zhu, L. M., Zhang, J., Zhai, D. G., et al. (2019). Gold deposit types and mineralization in the West Qinling region. *Earth Science Frontiers*, *26*(5), 1–16. https://doi.org/10.13745/j.esf.sf.2019.8.15

Liu, S. N., & Wang, Y. (2023). Origin of the Songpan-Garze Terrane on the northeastern Tibetan Plateau, eastern segment of the Tethyan tectonic domain: A Middle Permian–Early Triassic intracontinental rifting system. *Geological Society of America Bulletin*, *135*(7–8), 1993–2014. https://doi.org/10.1130/B36468.1

Liu, X. C., Wu, Y., Gao, S., Wang, J., Peng, M., Gong, H., et al. (2011). Zircon U–Pb and Hf evidence for coupled subduction of oceanic and continental crust during the Carboniferous in the Huwan shear zone, western Dabie orogen, central China. *Journal of Metamorphic Geology*, *29*(2), 233–249. https://doi.org/10.1111/j.1525-1314.2010.00914.x

Liu, Y., Xiao, W. J., Hu, J., Ren, Z. H., Sang, M., & Mao, Q. G. (2025). Provenance and tectonic setting of the Songpan-Ganzi complex in the Tibetan Plateau: Insights from the Monte Carlo unmixing modeling with age spectra and isotopes. *Tectonics*, *44*(4), e2024TC008624. https://doi.org/10.1029/2024TC008624

Liu, Z. Q., Pei, X. Z., Li, R. B., Li, Z. C., Zhang, X. F., Liu, Z. G., et al. (2011). LA-ICP-MS zircon U-Pb geochronology of the two suites of ophiolites at the Buqingshan area of the A'nyemaqen Orogenic Belt in the southern margin of East Kunlun and its tectonic implication. *Acta Geologica Sinica*, *85*, 185–194. https://doi.org/10.1111/j.1755-6724.2011.00204.x

Luo, B. J., Zhang, H. F., & Lü, X. B. (2012). U–Pb zircon dating, geochemical and Sr–Nd–Hf isotopic compositions of early Indosinian intrusive rocks in West Qinling, central China: Petrogenesis and tectonic implications. *Contributions to Mineralogy and Petrology*, *164*(4), 551–569. https://doi.org/10.1007/s00410-012-0748-2

Meng, Q. R., Qu, H. J., & Hu, J. M. (2007). Triassic deep-marine sedimentation in the western Qinling and Songpan terrane. *Science in China Series D: Earth Sciences*, *50*(Suppl 2), 246–263. https://doi.org/10.1007/s11430-007-6009-y

Meng, Q. R., & Zhang, G. W. (1999). Timing of collision of the North and South China blocks: Controversy and reconciliation. *Geology*, *27*(2), 123–126. https://doi.org/10.1130/0091-7613(1999)027<0123:TOCOTN>2.3.CO;2

Mooney, W., Wang, Y., Yuan, X., & Okaya, N. (2005). Crustal structure of the NE Tibetan plateau, China, from deep crustal seismic profiling data. *AGU Fall Meeting Abstracts*, *2005*, T41A–1275.

Muntean, J. L., Cline, J. S., Simon, A. C., & Longo, A. A. (2011). Magmatic-hydrothermal origin of Nevada's Carlin-type gold deposits. *Nature Geoscience*, *4*(2), 122–127. https://doi.org/10.1038/ngeo1064

Mutti, E. (1985). Turbidite systems and their relations to depositional sequences. In *Provenance of arenites* (pp. 65–93). Springer Netherlands.

Nie, S., Yin, A., Rowley, D. B., & Jin, Y. (1994). Exhumation of the Dabie Shan ultra-high-pressure rocks and accumulation of the Songpan-Ganzi flysch sequence, central China. *Geology*, *22*(11), 999–1002. https://doi.org/10.1130/0091-7613(1994)022<0999:EOTDSU>2.3.CO;2

Pan, Y. (2026). The tectonic debate on the Songpan-Ganzi domain: Remnant ocean basin or hyper-extended continental margin? [Dataset]. *Figshare*. https://doi.org/10.6084/m9.figshare.31260439

Pan, Y. D., & Hu, X. M. (2024). A database of detrital zircon U–Pb geochronology and Hf isotopes from the Songpan–Ganzi and Western Qinling terranes. *Geoscience Data Journal*, gdj3.195. https://doi.org/10.1002/gdj3.195

Pan, Z., Sun, F., Cong, Z., Tian, N., Xin, W., Wang, L., et al. (2022). Petrogenesis and tectonic implications of the Triassic granitoids in the Ela Mountain area of the East Kunlun Orogenic Belt. *Minerals*, *12*(7), 880. https://doi.org/10.3390/min12070880

Peng, H., Yin, C., Zhong, Y., Yang, Y. M., Xu, L., Luo, Y., et al. (2021). A new scale shoal-forming model and natural gas exploration implications in Feixianguan Formation, northwestern Sichuan Basin, China. *Energy Exploration & Exploitation*, *39*(6), 1857–1877. https://doi.org/10.1177/01445987211005219

Pullen, A., Kapp, P., Gehrels, G. E., Vervoort, J. D., & Ding, L. (2008). Triassic continental subduction in central Tibet and Mediterranean-style closure of the Paleo-Tethys Ocean. *Geology*, *36*(5), 351–354. https://doi.org/10.1130/G24435A.1

Qian, Q., & Wang, Y. (2025). Episodic tectonism, metamorphism, magmatism, mineralization and mass mortality in eastern China (and adjacent regions) during the Yanshanian movement: Consequences of major global plate reorganizations during the main episodes of Pangea breakup? *Earth-Science Reviews*, *265*, 105107. https://doi.org/10.1016/j.earscirev.2025.105107

Qiu, K. F., & Deng, J. (2017). Petrogenesis of granitoids in the Dewulu skarn copper deposit:implications for the evolution of the Paleotethys Ocean and mineralization in Western Qinling, China. *Ore Geology Reviews*, *90*, 1078–1098. https://doi.org/10.1016/j.oregeorev.2016.09.027

Qiu, K. F., Taylor, R. D., Song, Y. H., Yu, H. C., Song, K. R., & Li, N. (2016). Geologic and geochemical insights into the formation of the Taiyangshan porphyry copper-molybdenum de-posit, Western Qinling Orogenic Belt, China. *Gondwana Research*, *35*, 40–58. https://doi.org/10.1016/j.gr.2016.03.014

Raimondo, T., Hand, M., & Collins, W. J. (2014). Compressional intracontinental orogens: Ancient and modern perspectives. *Earth-Science Reviews*, *130*, 128–153. https://doi.org/10.1016/j.earscirev.2013.11.005

Sengör, A. M. C. (1984). *The Cimmeride orogenic system and the tectonics of Eurasia* (Vol. 195, p. 82). Geological Society America Special Paper. https://doi.org/10.1130/SPE195-p1

Şengor, A. M. C., & Hsü, K. J. (1984). The Cimmerides of eastern Asia: History of the eastern end of PalaeoTethys. *Memoire Société Geologie de France NouvelleSérie*, *147*, 139–167.

Sharman, G. R., Sharman, J. P., & Sylvester, Z. (2018). detritalPy: A python-based toolset for visualizing and analysing detrital geothermochronologic data. *Depositional Record*, *4*(2), 202–215. https://doi.org/10.1002/dep2.45

Shi, Y., Liu, X. L. X., Peng, C., Hou, Z., Zhou, A., & Wang, J. (2022). Tectonic evolution of the Southern Dabie orogenic Belt, China: Insights from peak P–T conditions and U–Pb zircon dating of the susong metamorphic complex. *Minerals*, *12*(10), 1201. https://doi.org/10.3390/min12101201

Silva, D., Piazolo, S., Daczko, N. R., Houseman, G., Raimondo, T., & Evans, L. (2018). Intracontinental orogeny enhanced by far-field extension and local weak crust. *Tectonics*, *37*(12), 4421–4443. https://doi.org/10.1029/2018TC005106

Song, S. G., Wang, M. J., Wang, C., & Niu, Y. L. (2015). Magmatism during continental collision, subduction, exhumation and mountain collapse in collisional orogenic belts and continental net growth: A perspective. *Science China Earth Sciences*, *58*(8), 1284–1304. https://doi.org/10.1007/s11430-015-5102-x

Song, S. Y., Zhou, M. F., Cao, Z. M., & Robinson, P. T. (2004). Late Permian rifting of the South China craton caused by the Emeishan mantle plume? *Journal of the Geological Society of London*, *161*(5), 773–781. https://doi.org/10.1144/0016-764903-135

Tang, Y., Yin, A., Xu, X., An, K. X., & Zhang, Y. P. (2023). Tectonic evolution of the Triassic Songpan-Ganzi basin as constrained by a synthesis of multi-proxy provenance data. *Basin Research*, *35*(1), 28–60. https://doi.org/10.1111/bre.12703

Vermeesch, P. (2013). Multi-sample comparison of detrital age distributions. *Chemical Geology*, *341*, 140–146. https://doi.org/10.1016/j.chemgeo.2013.01.010

Vermeesch, P. (2021). Maximum depositional age estimation revisited. *Geoscience Frontiers*, *12*(2), 843–850. https://doi.org/10.1016/j.gsf.2020.08.008

Wang, F. C., Zheng, T., Qian, Y., Yu, X. F., & Qiao, J. F. (2023). Scissors-type closure of the A'nyemaqen Ocean: Geochronological and geochemical constraints of Late Permian-Triassic granitoids in the East Kunlun Orogen. *Geological Journal*, *58*(2), 883–902. https://doi.org/10.1002/gj.4632

Wang, H., Gao, R., Li, Q., Li, W., Hou, H., Kuang, C., et al. (2014). Deep seismic reflection profiling in the Songpan-west Qinling-Linxia basin of the Qinghai-Tibet plateau: Data acquisition, data processing and preliminary interpretations. *Chinese Journal of Geophysics*, *57*, 1451–1461.

Wang, H. Q., Zhu, Y. H., Lin, Q. X., Li, Y. L., & Wang, K. (2010). LA-ICP-MS zircon U–Pb dating of the gabbro from Longwu Gorge ophiolite, Jianzha-Tongren area, Qinghai, China and its geological significance. *Geological Bulletin of China*, *29*, 86–92.

Wang, T. T., Ran, B., Wang, C. S., Li, X. H., Liu, S. G., Li, Z. W., et al. (2024). Evidence of detrital spinel geochemistry for depositional response to the Paleo-Tethyan closure recorded in the Songpan-Ganzi Terrane, eastern Tibetan Plateau. *Journal of Asian Earth Sciences*, *270*, 106191. https://doi.org/10.1016/j.jseaes.2024.106191

Wang, X., Wang, T., Castro, A., Ke, C. H., Yang, Y., & Hu, N. G. (2018). Magmatic evolution and source of a Proterozoic rapakivi granite complex in the North China Craton: New evidence from zircon U– Pb ages, mineral compositions, and geochemistry. *Journal of Asian Earth Sciences*, *167*, 165–180. https://doi.org/10.1016/j.jseaes.2017.10.019

Wang, X. X., Wang, T., & Zhang, C. L. (2013). Neoproterozoic, Paleozoic, and Mesozoic granitoid magmatism in the Qinling Orogen, China: Constraints on orogenic process. *Journal of Asian Earth Sciences*, *72*, 129–151. https://doi.org/10.1016/j.jseaes.2012.11.037

Wang, Y., Shi, K., & Liu, B. (2023). Sedimentary structures of microbial carbonates in the fourth member of the Middle Triassic Leikoupo Formation, Western Sichuan Basin, China. *Scientific Reports*, *13*(1), 2300. https://doi.org/10.1038/s41598-023-28211-0

Weislogel, A. L., Graham, S., Chang, E., Wooden, J., & Gehrels, G. (2010). Detrital zircon provenance from three turbidite depocenters of the Middle–Upper Triassic Songpan-Ganzi complex, central China: Record of collisional tectonics, erosional exhumation, and sediment production. *Geological Society of America Bulletin*, *122*(11–12), 2041–2062. https://doi.org/10.1130/B26606.1

Weislogel, A. L., Graham, S. A., Chang, E. Z., Wooden, J. L., Gehrels, G. E., & Yang, H. (2006). Detrital zircon provenance of the Late Triassic Songpan-Ganzi complex: Sedimentary record of collision of the North and South China blocks. *Geology*, *34*(2), 97–100. https://doi.org/10.1130/G21929.1

Wiedenbeck, M., Hanchar, J. M., Peck, W. H., Sylvester, B., Valley, J., Whitehouse, M., et al. (2004). Further characterisation of the 91500 zircon crystal. *Geostandards and Geoanalytical Research*, *28*(1), 9–39. https://doi.org/10.1111/j.1751-908X.2004.tb01041.x

Xia, R., Min, Q., Wang, C., & Li, W. (2014). The genesis of the ore-bearing porphyry of the Tuoketuo porphyry Cu-Au (Mo) deposit in the East Kunlun, Qinghai Province: Constraints from zircon U-Pb geochronology and geochemistry. *Journal of Jilin University (Earth Science Edition)*, *44*(5), 1502–1524. https://doi.org/10.13278/j.cnki.jjuese.201405110

Xia, T. L., Li, K. Z., Hu, L. S., Zhao, Z. L., Huang, Y., Ma, Q. L., & Q, L. (2024). A database of detrital zircon geochronology ages of Cambrian to Paleogene deposits in South China. *Geoscience Data Journal*, *11*(4), 405–413. https://doi.org/10.1002/gdj3.196

Xu, Z., Hou, L., & Wang, Z. (1992). *Orogenic Process of the Songpan–Garze Orogenic Belt of China (in Chinese with English abstract)* (pp. 1–190). Geological Publishing House.

Xu, Z., Wang, Z., & Hou, L. (1991). New advances in the tectonic studies of the Songpan-Garzê orogenic belt. *Geology in China*(12), 14–16.

Xue, W. W., Hu, X. M., Garzanti, E., Ma, A. L., Lai, W., & Li, C. (2023). Discriminating Qiangtang, Lhasa, and Himalayan sediment sources in the Tibetan Plateau by detrital-zircon U-Pb age and Hf isotope facies. *Earth-Science Reviews*, *236*, 104271. https://doi.org/10.1016/j.earscirev.2022.104271

Yan, Z., Aitchison, J. C., Fu, C., Guo, X., Xia, W., & Niu, M. (2016). Devonian sedimentation in the Xiqingshan Mountains: Implications for paleogeographic reconstructions of the SW Qinling Orogen. *Sedimentary Geology*, *343*, 1–17. https://doi.org/10.1016/j.sedgeo.2016.07.009

Yan, Z., Fu, C. L., Aitchison, J. C., Buckman, S., Niu, M. L., & Cao, B. (2020). Triassic turbidites in the West Qinling Mountains, NW China: Part of the collisional Songpan-Ganzi Basin or an active forearc basin? *Journal of Asian Earth Sciences*, *194*, 104366. https://doi.org/10.1016/j.jseaes.2020.104366

Yang, F. Q., & Wang, Z. P. (1995). Reconstruction of the Permian paleo-ocean of the Qinling orogenic belt. *Earth Science - Journal of China University of Geosciences*, *20*(6), 641–647.

Yang, J. S., Shi, R. D., Wu, C. L., Wang, X. B., & Robinson, P. T. (2009). Dur'ngoi ophiolite in East Kunlun, Northeast Tibetan plateau: Evidence for paleo-tethyan suture in Northwest China. *Journal of Earth Science*, *20*(2), 303–331. https://doi.org/10.1007/s12583-009-0027-y

Yang, W., Tang, W., Yang, J. H., Zhang, H. Y., & Du, Y. S. (2025). Middle Triassic humidification in Southern North China linked to northward propagation of Qinling Orogenic Belt. *Palaeogeography, Palaeoclimatology, Palaeoecology*, *669*, 112948. https://doi.org/10.1016/j.palaeo.2025.112948

Yang, W. T., Li, Q., Yang, J. H., Fang, T., & Ma, R. (2023). Dataset of detrital zircon U–Pb ages and Hf isotopic compositions for the late Paleozoic–Mesozoic strata in the North China block. *Geoscience Data Journal*, gdj3.211. https://doi.org/10.1002/gdj3.211

Yin, A., & Harrison, T. M. (2000). Geologic evolution of the Himalayan-Tibetan orogen. *Annual Review of Earth and Planetary Sciences*, *28*(1), 211–280. https://doi.org/10.1146/annurev.earth.28.1.211

Yin, A., & Nie, S. (1993). An indentation model for the North and South China collision and the development of the Tan-Lu and Honam fault systems, eastern Asia. *Tectonics*, *12*(4), 801–813. https://doi.org/10.1029/93TC00313

Yin, H. F. (1992). *The Triassic of Qinling mountains and neighboring areas*. Press of the China University of geosciences.

Yin, H. F., & Peng, Y. Q. (1995). Evolution of the Phanerozoic paleo-ocean of Qinling. *Earth Science*, *20*(6), 605–611.

Yu, H. C., Qiu, K. F., Pirajno, F., Zhang, P. Z., & Dong, W. Q. (2022). Revisiting Phanerozoic evolution of the Qinling Orogen (East Tethys) with perspectives of detrital zircon. *Gondwana Research*, *103*, 426–444. https://doi.org/10.1016/j.gr.2021.10.022

Yu, X., Li, J., Jin, X., Zhao, S., He, C., & Zhu, Y. (2024). Monazite U-Th-Pb and sericite Rb-Sr dating of the Xiajiadian black shale-hosted gold deposit in the Qinling orogen, central China: Implications for regional gold metallogeny. *Science China Earth Sciences*, *67*(8), 2478–2494. https://doi.org/10.1007/s11430-023-1244-6

Zhan, Q. Y., Zhu, D. C., Wang, Q., Cawood, P. A., Xie, J. C., Liu, X., et al. (2021). Imaging the Late Triassic lithospheric architecture of the Yidun Terrane, eastern Tibetan Plateau: Observations and interpretations. *Geological Society of America Bulletin*, *133*(11–12), 2279–2290. https://doi.org/10.1130/B35778.1

Zhang, K. J. (2001). Is the Songpan-Ganzi terrane (central China) really underlain by oceanic crust? *Journal of the Geological Society of India*, *57*(3), 223–230. https://doi.org/10.17491/jgsi/2001/570303

Zhang, Q., Zhou, D., Zhao, D., Huang, Z., Han, S., Jia, X., & Dong, J. (1994). Ophiolites of the Hengduan Mountains, China: Characteristics and tectonic settings. *Journal of Southeast Asian Earth Sciences*, *9*(4), 335–344. https://doi.org/10.1016/0743-9547(94)90044-2

Zhang, Y. X., Zeng, L., Zhang, K. J., Li, Z. W., Wang, C. S., & Guo, T. L. (2014). Late Palaeozoic and early Mesozoic tectonic and palaeogeographic evolution of central China: Evidence from U–Pb and Lu–Hf isotope systematics of detrital zircons from the western Qinling region. *International Geology Review*, *56*(3), 351–392. https://doi.org/10.1080/00206814.2013.864475

Zhao, Z. G., Huang, X., Zhang, X. H., Yang, B., Chen, Z. Q., & Xiong, F. H. (2016). Permian radiolarians from the a'nyemaqen mélange zone in the Huashixia area of Madoi County, Qinghai Province, Western China, and their implications on regional tectonism. *Journal of Earth Science*, *27*(4), 623–630. https://doi.org/10.1007/s12583-016-0711-7

Zhao, Z. G., Yang, B., Huang, X., Zhang, X. H., Yang, B., & Wang, J. (2013). Discovery of the Middle Permian fusulinids from the Changshitou Mountain in Maduo, Qinghai and its geological significance. *Journal of Stratigraphy*, *37*(3), 292–296.

Zheng, Q., Hu, J., Gurnis, M., Chen, L., Shi, Y. L., Bao, X. Y., & Yang, Y. (2025). Ongoing India–Eurasia collision predominantly driven by Sumatra–Java slab pull. *Nature Geoscience*, *18*(9), 909–915. https://doi.org/10.1038/s41561-025-01771-8

Zhou, D., & Graham, S. A. (1995). The Songpan-Ganzi complex of the West Qinling Shan as a Triassic remnant ocean basin. *World and Regional Geology*, *1*(8), 281–299.